NASA Contractor Report 4717

Final Report on Nimbus–7 TOMS Version 7 Calibration

C. G. Wellemeyer, S. L. Taylor, G. Jaross, M. T. DeLand,
C. J. Seftor, G. Labow, T. J. Swissler, and R. P. Cebula

CONTRACT NAS5-31755
MARCH 1996

NASA Contractor Report 4717

Final Report on Nimbus–7 TOMS Version 7 Calibration

C. G. Wellemeyer, S. L. Taylor, G. Jaross, M. T. DeLand,
C. J. Seftor, G. Labow, T. J. Swissler, and R. P. Cebula
Hughes STX
Greenbelt, Maryland

Prepared for
Goddard Space Flight Center
under Contract NAS5-31755

National Aeronautics
and Space Administration

**Scientific and Technical
Information Branch**

1996

This publication is available from the NASA Center for AeroSpace Information,
800 Elkridge Landing Road, Linthicum Heights, MD 21090-2934, (301) 621-0390.

TABLE OF CONTENTS

LIST OF FIGURES

LIST OF FIGURES (Continued)

LIST OF TABLES

1.0 INTRODUCTION

1.1 Background

The Total Ozone Mapping Spectrometer (TOMS) experiment [*Heath et al., 1978*] on board the Nimbus–7 satellite provided daily global coverage of total column ozone by measuring Earth's ultraviolet backscatter in six 1-nm bands. The nominal wavelengths measured are 312, 317, 331, 340, 360, and 380 nm. The longer wavelengths are used to monitor the reflective properties of the surface underlying the atmosphere, and the shorter wavelengths are used to measure total column ozone. The experiment used a single monochromator and scanning mirror to sample the Earth's radiation at 35 sample points in three-degree intervals along a line perpendicular to the orbital plane. The spacecraft moves from south to north during the sunlit portions of its near polar orbit. The Earth radiances are normalized using solar measurements made near the northern terminator.

The TOMS was launched aboard Nimbus–7 on October 28, 1978, and ceased to function on May 6, 1993. This length of data record makes the TOMS useful for trend studies of total ozone over a period when unprecedented changes in global ozone have been measured [*Stolarski et al., 1992, Herman and Larko, 1993, Gleason et al., 1993, and Schoeberl et al., 1993*]. The previous Version 6 calibration of TOMS was determined through 1989 [*Herman et al., 1991*], and then extrapolated through the end of the experiment. The need to redetermine the calibration of TOMS during the extrapolated period was anticipated, and large changes in the instrument sensitivity toward the end of the data record have made it necessary. A Version 7 release of the TOMS data has been carried out to update the TOMS instrument characterization, and to make some improvements to the TOMS ozone retrieval. The Version 7 data should be used in all future studies involving TOMS ozone or reflectivity. The data are archived and distributed by the Distributed Active Archive Center (DAAC) at the Goddard Space Flight Center in Greenbelt, Maryland.

The TOMS retrieval algorithm uses differential absorption across a pair of wavelengths; one strongly absorbed by ozone, and one very weakly absorbed [*McPeters et al., 1993*]. In the Version 7 algorithm, a third non-absorbing wavelength is used to identify possible wavelength dependence in the reflective properties of the underlying surface [*McPeters et al., 1996*]. Measured radiances are compared with theoretical radiances calculated for a set of possible ozone amounts and distributions at the viewing geometry and estimated surface conditions to infer total ozone amount. The total ozone algorithm is only very weakly dependent on the absolute calibration of the individual wavelength channels, but is strongly dependent on their relative calibration.

For past TOMS calibrations, including Version 6, the Earth radiance measurements were normalized using periodic solar measurements made near the northern terminator by deploying a ground aluminum solar diffuser plate to reflect sunlight into the instrument. When the ratio of the Earth radiance to the solar irradiance was calculated for use in the algorithm, the instrument changes canceled except for any changes in the reflective properties of the solar diffuser. So, the problem of long-term calibration of the normalized Earth radiance measured by TOMS reduced to the characterization of changes in the reflective properties of the solar diffuser [*Cebula et al., 1988*]. In the current study however, the diffuser characterization is removed from the problem of long-term calibration entirely. This is accomplished by assuming that the solar output has not changed at the TOMS wavelengths over the course of the experiment, and normalizing the Earth radiance measurement using only the initial solar irradiance measurement. Using this approach, it is the instrument changes that must be characterized in order to achieve long-term calibration stability.

Because of a drifting local equator crossing time in the Nimbus–7 orbit, the solar azimuth angles on the TOMS diffuser were periodically beyond the range of all prelaunch calibration data during the last three years of the experiment. In addition, partial shadowing of the diffuser began to occur during the last two years of operation. Therefore, any reliance on the solar measurements at the end of the data record has been minimized in the Version 7 calibration analysis.

For the Version 7 calibration, we have developed an improved method called "spectral discrimination" to calibrate the longer reflectivity wavelengths of TOMS. For the shorter ozone wavelengths we have implemented a straight-forward approach of using a simple quadratic fit in wavelength across the reflectivity channels to extrapolate the

calibrations to 317 and 312 nm. This approach is validated using the Pair Justification Method (PJM), the technique used in the Version 6 calibration.

1.2 Overview

In Section 2, Basic Measurement, the radiance measurement made by TOMS is described in detail, and the sensitivity of the ozone retrieval algorithm to errors in the radiance measurement is discussed. Section 3, Time-Dependent Radiance Calibration, describes the internal methods used to determine the Version 7 TOMS time-dependent radiance calibration. Some of the results obtained in later sections depend on the TOMS companion instrument, Solar Backscatter Utlra Violet (SBUV), for validation of the calibration procedures. In Section 4, TOMS-SBUV Comparisons, the calculation of coincident radiances between the two co-aligned instruments is discussed and some results are presented. In Section 5, TOMS Wavelength Scale Adjustments, errors in the original wavelength calibration of Nimbus–7 are found to explain most of the initial ozone bias between TOMS and SBUV. In Section 6, Initial Calibration Adjustments, adjustments to the TOMS initial calibration intended to bring it into closer agreement with other satellite measurements are discussed. Section 7, Impact of Chopper Non-Synchronization, describes small adjustments for changes in synchronization state and errors associated with the occurrence of non-synchronization. In Section 8, Other Instrument Performance Issues, evidence of hysteresis in the TOMS and possible signal level dependence in the TOMS relative to SBUV are presented. Section 9, Combined Uncertainties, summarizes the TOMS calibration errors, and in the last section, our conclusions are presented.

2.0 BASIC MEASUREMENT

2.1 Radiance Measurement

The TOMS instrument is designed to measure the radiant intensity of a diffuse source, the sunlit Earth, or a diffuse reflector illuminated by the Sun. For a given intensity $I(\lambda)$ in watt/m^2/nm/sr, the output instrument count rate C in gain range i at a particular wavelength band B is given by:

$$C_B = A\ \Delta\Omega g_i \int I(\lambda)\eta(\lambda)T\ (\lambda)S\ (\lambda-\lambda_B)\,d\lambda \tag{1}$$

where,

- A = entrance aperture area
- $\Delta\Omega$ = instrument Field of View (FOV) solid angle
- g_i = channel gain for gain range i=1,2,3,4
- $\eta(\lambda)$ = Photomultiplier tube (PMT) detection efficiency
- $T(\lambda)$ = Instrument transmission
- $S(\lambda)$ = Instrument bandpass
- λ_B = Central wavelength of band B=1,2,...,6.

The measurement of solar flux, (F_λ), is the same except that the measured intensity is reflected off of the solar diffuser plate so that the angular or goniometric dependence of its reflectivity must be taken into account:

$$I\ (\lambda) = F(\lambda)\cos(\theta_I)\ \ \rho(\theta_I,\theta_S\phi,\lambda) \tag{2}$$

where,

- $\rho(\theta_I, \theta_S, \phi, \lambda)$ = Bi-directional Reflectivity Distribution Function (BRDF) of the diffuser plate
- θ_I = Aperture elevation angle with respect to the diffuser
- θ_S = Solar elevation angle with respect to the diffuser
- ϕ = Solar azimuth angle with respect to the diffuser
- λ = Wavelength

We assume that the instrument transmission and PMT detector efficiency vary slowly across the 1-nm triangular slit function so that:

$$C_B = A\ \Delta\Omega g_i\ \eta_B T_B \int I(\lambda)\ S(\lambda-\lambda_B)\,d\lambda \tag{3}$$

The error in this assumption can be estimated based on the wavelength dependence of the prelaunch calibration coefficients relating measured counts to intensity, and the instrument changes estimated in Section 3.0. At worst case, the assumption is in error by 1 percent/nm at launch, and 2 percent/nm at the end of the record. The impact of this error is reduced by the mean value theorem, indicating that some weighted mean value of these parameters can be taken out of the integral. A similar assumption is made for the solar measurement with worst case errors of 2 percent/nm at launch and 4 percent/nm at the end of the record.

If the measurement system is linear, the counts are proportional to the number of incident photons, and the ratio of counts measured in Earth view to solar view is:

$$\frac{C_E}{C_S} = \frac{g_i}{g_j}\,\frac{1}{\cos(\theta_I)\ \rho(\theta_I,\theta_S,\phi)}\,\frac{\bar{I}}{\bar{F}} \tag{4}$$

Note that the Earth radiance and solar measurements may not be in the same gain range. Thus, for a linear system, the initial calibration of the instrument requires knowledge of the gain range ratios and the BRDF of the solar diffuser. In addition, to convert the measured I/F into ozone, we need to know the band center wavelength (λ_B) and the bandpass $S(\lambda)$.

For the time-dependent calibration of the instrument, we consider only the Earth radiance measurement, which when integrated over wavelength becomes:

$$C_E = g_i A \Delta \Omega \eta_B T_B \bar{I} \tag{5}$$

The accuracy of this measurement depends on knowledge of some reference gain, but the precision depends only on knowledge of the inter-range ratios. We assume that the entrance aperture (A) and the instrument FOV solid angle ($\Delta\Omega$) are constant. The inter-range ratios of the electronic gain (g_i) are monitored by analyzing the discontinuity in signal at the gain switching points. We have verified these to be stable to better than 0.5 percent. The time dependence of the reference gain is an unknown, and must be lumped with the PMT detection efficiency (η_B), and the instrument transmission (T) into an instrument change factor that needs to be determined in order to fully calibrate the TOMS radiances. The technique used to accomplish this is described in Section 3, Radiance Calibration.

2.2 Ozone Sensitivity

A basic understanding of the algorithmic sensitivity to instrument errors is fundamental to any calibration analysis. In the TOMS Version 7 algorithm, the measured radiances are compared to theoretical radiances to derive ozone. In order to calculate theoretical radiances, the effective surface reflectivity must be known. This quantity is the reflectivity of a Lambertian surface at the reflecting surface pressure that is consistent with the measured radiance. The longest TOMS channel at 380 nm that has no sensitivity to ozone is used to derive this quantity, which may be referred to below as simply the reflectivity or surface reflectivity. The assumption in previous algorithms has been that the surface reflectivity is independent of wavelength, but in the Version 7 algorithm a linear dependence is assumed. Using an initial estimate of total ozone and the reflectivity derived from the 380-nm channel, initial residues are computed as the difference between the measured radiances and theoretical radiances calculated using the initial ozone value. Making the assumption of linear dependence in the effective surface reflectivity, the initial residues can be written as:

$$r_\lambda = s_\lambda (\Omega - \Omega_0) + a + b\lambda \tag{6}$$

where

- s_λ = the theoretical sensitivity of the radiances to changes in ozone
- Ω_0 = the initial ozone estimate
- Ω = the solution ozone
- λ = the wavelength
- a = a zeroth order constant
- b = a first order constant

Since the effective reflectivity is derived using the 380 nm channel, the residue at 380 nm is zero. Since the ozone sensitivity at 380 nm is also zero, Equation 6 can be written for 380 nm and solved for the zeroth order constant a. Two more equations can be written for a pair of wavelengths (λ_1 and λ_2), and solved for the remaining two unknowns, b and Ω giving:

$$\Omega = \Omega_0 + \frac{r_1 \delta\lambda_2 - r_2 \delta\lambda_1}{s_1 \delta\lambda_2 - s_2 \delta\lambda_1} \tag{7}$$

where the subscripts (1 and 2) refer to the wavelengths in the pair, and:

$\delta\lambda$ = the difference between a given wavelength and 380 nm (λ - 380).

Equation 7 is referred to as the triplet formulation, because it is based on the measurements at three channels. However, it still relies on the differential absorption across a pair of wavelengths to infer ozone. The third wavelength is simply used to estimate any wavelength dependence in the derived surface reflectivity. No assumption is made as to the source of this dependence; it may be the result of surface reflectivity effects, atmospheric effects, or instrument calibration errors. The wavelength pairs used for the Nimbus–7 TOMS are designated A-pair (312–331 nm), B-pair (317–331 nm), and C-pair (331–340 nm). Since these wavelengths are relatively closer to each other than to 380 nm ($\delta\lambda_1 \approx \delta\lambda_2$), Equation 7 is dominated by the difference in residues at the two wavelengths in the pair. This means that the derived ozone is sensitive to wavelength dependent calibration errors that change r_2 relative to r_1, but relatively insensitive to calibration errors that are independent of wavelength. This is illustrated in Figure 1, which shows the ozone and reflectivity errors that result from a wavelength independent error of 10 percent in measured radiance. The errors in derived ozone are all less than 2 percent, but the fractional reflectivity error can be larger than 0.20 at very high path lengths. Over most of the globe, the range of reflectivity errors is large. This is because the reflectivity sensitivity to calibration errors is smaller for low reflectivity than it is for high reflectivity by about a factor of 3.

Because of the linear assumption adopted in Equation 6, calibration errors that are linear with wavelength have little or no effect on derived ozone. Such an error was used in a test similar to that illustrated in Figure 1 with an error of 10 percent at 312 nm and zero at 380 nm. It produced errors in ozone that were all less than 1 percent everywhere. To induce a significant error in derived ozone, a calibration error must have some second order dependence in wavelength. Figure 2 shows the results of a purely second order calibration error (parabolic in wavelength) that is 10 percent at 312 nm and zero at 380 nm. The linear assumption reduces the impact of an error of this type, but of course does not remove it entirely. The differences between the quadratic calibration error and the corrective linear assumption in the case of the A-pair, B-pair, and C-pair wavelengths are approximately 2.8 percent, 1.9 percent, and 1.0 percent respectively. Note that the closer the wavelengths in the pair, the smaller the impact. The longer wavelength pairs are used at longer optical path lengths. The A-pair is used over most of the globe. It is used almost exclusively over the latitude range of 60° S to 55° N in Figure 2. The B-pair is used at high path lengths. It is more sensitive to calibration errors than the A-pair, but its calibration error is better compensated for by the linear assumption because of its closer spacing in wavelength. This results in the slight reduction in the main cluster of errors seen in Figure 2 at high latitudes. The C-pair is only used at very high path lengths, and though its calibration error is well compensated by the linear assumption, its ozone sensitivity is quite low. The C-pair errors are clustered separately at high latitudes in the range of 2–6 percent. The reflectivity error is zero at all latitudes, since the radiance error was zero at 380 nm.

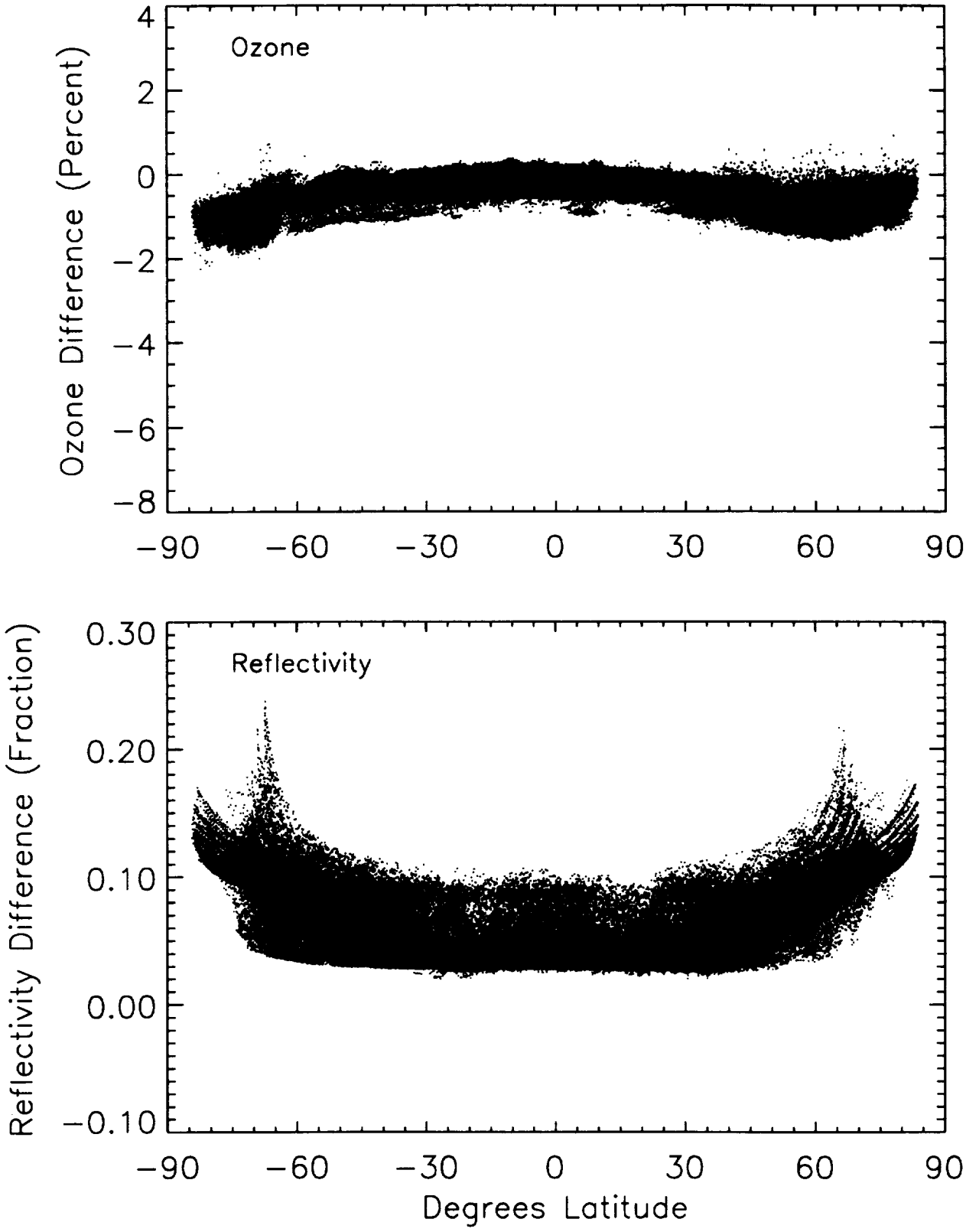

Figure 1. TOMS ozone and reflectivity errors resulting from a radiance error that is independent of wavelength. Calculated for an error of 10 percent on the sample day March 20, 1979.

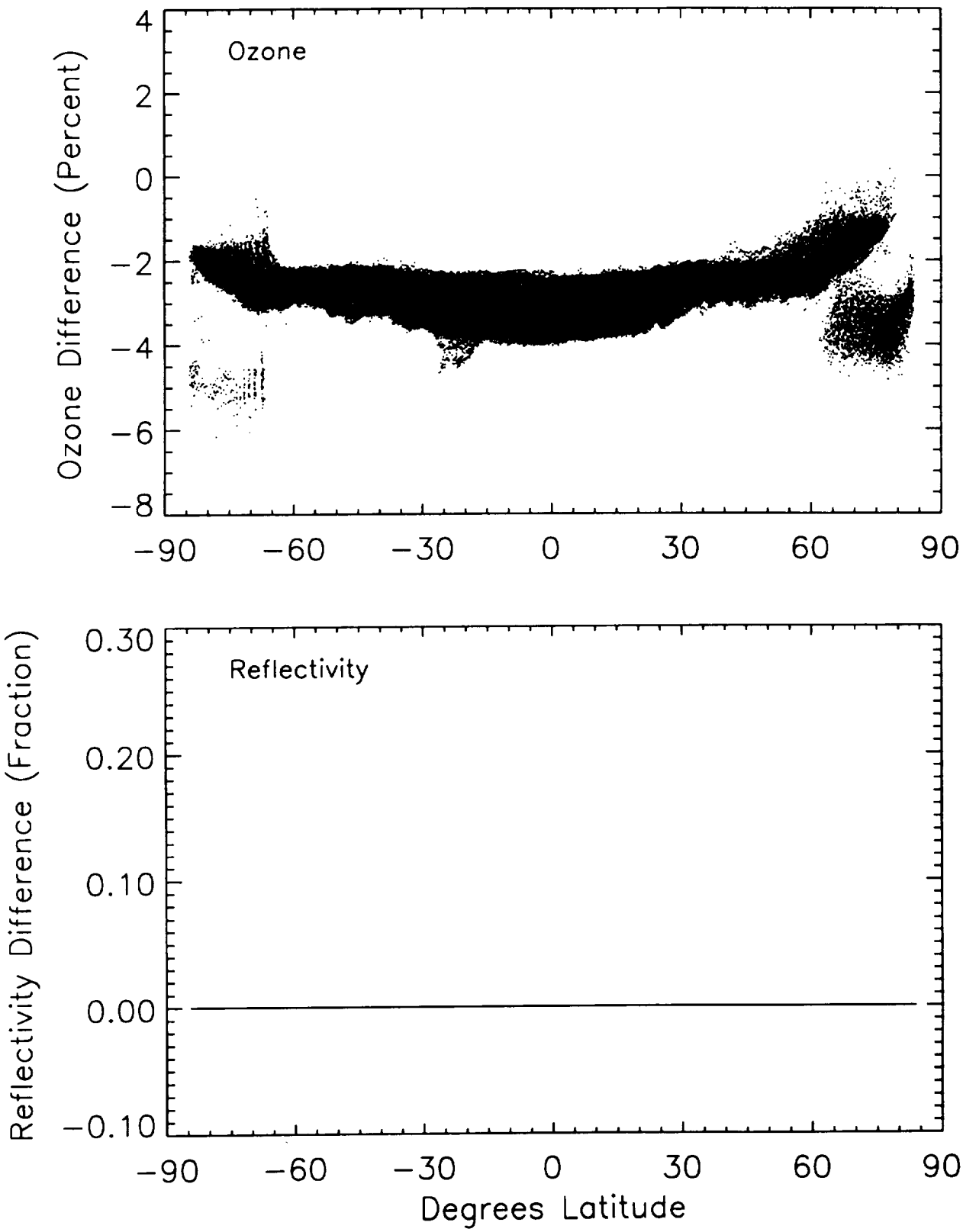

Figure 2. TOMS ozone and reflectivity errors resulting from a radiance error that is quadratic in wavelength. Calculated for an error of 10 percent at 312 nm and 0 percent at 380 nm on the sample day March 20, 1979

3.0 TIME-DEPENDENT RADIANCE CALIBRATION

3.1 Background

Figure 3 shows time series of daily average solar flux measured by TOMS at six discrete wavelengths. These data have been corrected for the BRDF of the diffuser, as well as variations in Sun-Earth distance and normalized to the initial measurement. The solar output does not vary significantly at these wavelengths, so the structure and trend in the time series is due to the combination of instrument and diffuser change. The data in Figure 3 show strong wavelength dependence and an increasing rate of change in the second half of the record. The impact of the loss of synchronization between the TOMS chopper wheel and the counting electronics [*Fleig et al., 1986*] can be seen as sharp perturbations of order 1 percent starting in early 1984 and ending in late 1990. As described in Section 7.2, a correction for this effect is applied to the radiances used in this calibration procedure.

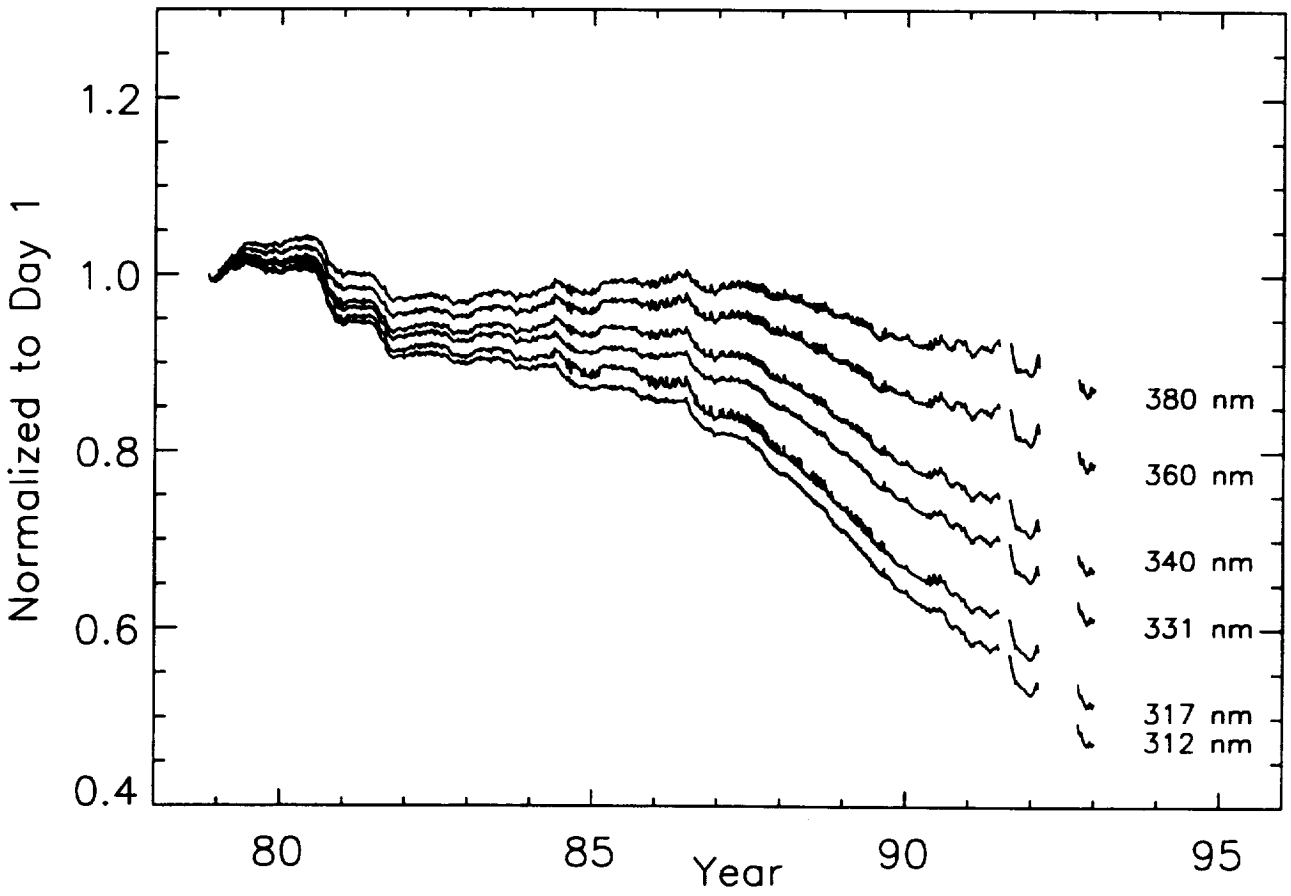

Figure 3. "Raw" solar flux as measured by the six Nimbus–7 TOMS wavelength channels normalized to the initial measurement. Changes include degradation of the solar diffuser plate as well as changes in the photomultiplier tube and instrument optics.

The changes illustrated in Figure 3 are due to degradation of the solar diffuser which is used only for the solar measurement, and to changes in other components of the instrument that are common to both solar and Earth measurements. These include changes in the instrument transmission, PMT efficiency, and the gain electronics, and will be referred to simply as the instrument change throughout the remainder of this discussion. Note also that the missing data and short-term variability at the end of the data record is largely due to errors in the characterization of the BRDF of the solar diffuser. This results from the drift of the Nimbus–7 orbit in the later years of the experiment, which leads to solar azimuth angles that are beyond the dynamic range of the prelaunch BRDF measurements. Even partial shadowing of the diffuser began to occur during the last two years of operation. Because of these problems, the solar measurements at the end of the data record are difficult to interpret.

Previous methods of long-term calibration for TOMS have focused directly on the characterization of the diffuser based on analysis of the solar measurements [*Cebula et al., 1988 and Herman et al., 1991*]. In the current study however, the diffuser characterization is removed from the problem of long-term calibration entirely. This is a fundamentally different strategy. It is accomplished by normalizing the Earth radiance measurement using only the initial solar irradiance measurement, and assuming that the solar output has not changed at the TOMS wavelengths over the course of the experiment. This assumption is good to better than 0.3 percent at the wavelengths measured by TOMS [*Schlesinger and Cebula, 1992 and Willson, et al., 1986*]. The geophysical parameters derived using such a normalization are affected by a calibration error that results from the instrument changes in TOMS exclusive of the diffuser. This error can be inferred from the behavior of the derived parameters as described below.

Figure 4 shows the "raw" equatorial Earth radiance measured by TOMS at each of the six wavelength channels. These data, which are smoothed because they are sampled only one day per month, are also corrected for variations in Sun-Earth distance and normalized to the initial measurement. The Sun-Earth distance correction takes into account the dependence of backscatter radiation on the solar flux. The Earth radiances are affected by geophysical variation in reflectivity and ozone. If we assume for the moment that these quantities are roughly constant in the equatorial region, these radiances provide a rough estimate of the TOMS instrument changes. The changes are essentially wavelength independent for the first eight or nine years of the experiment, and indicate an increase in instrument efficiency probably attributable to the PMT. The onset of wavelength dependence near the end of the data record is probably due to degradation of the TOMS optical components. Compared to the solar measurements, these changes show a simple wavelength independent behavior over the first half of the data record. Though the wavelength dependence increases dramatically during the second half of the record, the radiance measurements do provide a complete data record through the end of the experiment.

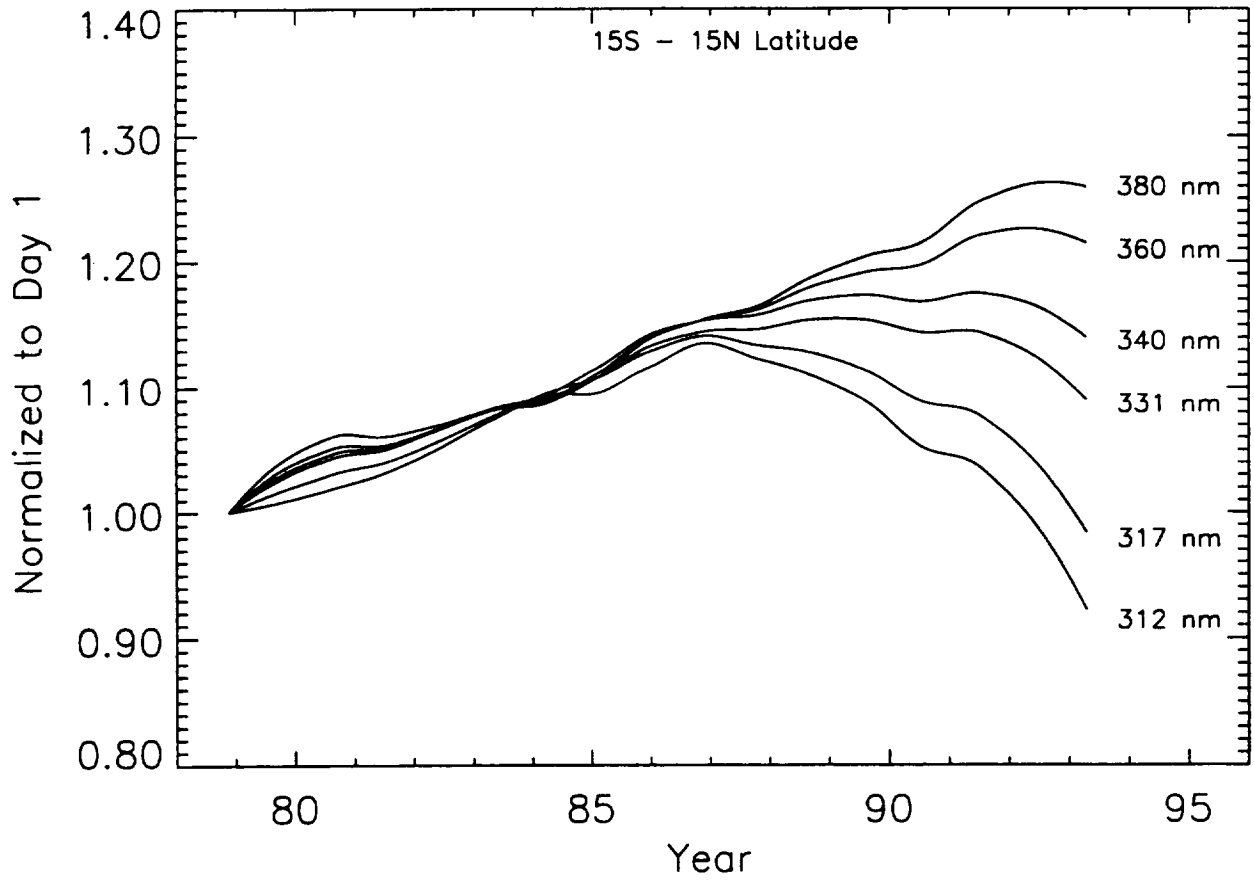

Figure 4. "Raw" Earth radiance as measured by six Nimbus–7 TOMS wavelength channels normalized to the initial measurement. Changes include changes in the photomultiplier tube, instrument optics, and geophysical changes in the Earth atmosphere. Data are sampled one day per month and smoothed.

3.2 Spectral Discrimination Method

The four longest TOMS wavelengths (380, 360, 340, and 331 nm) can be used to calculate surface reflectivity. Ozone absorption is accounted for in the two shortest reflectivity wavelengths, but accurate knowledge of the ozone amount is not needed to derive reflectivities from near nadir measurements in the tropics at low solar zenith angles. The derived reflectivity itself can be used to estimate calibration drift by finding areas of the Earth where geophysical variabilities are small. Previous studies have used minimum ocean reflectivity [*Herman et al., 1991*] and ice reflectivities over Greenland and Antarctica [*Jaross et al., 1995*] for this purpose. The accuracy of these methods is limited by residual geophysical variability caused by seasonal changes and angular dependence in the bi-directional surface reflectivity, cloud contamination, and aerosol effects. Stratospheric aerosols produced by Mt. Pinatubo are of particular concern since they were introduced near the end of the TOMS data record [*Bhartia et al., 1994*]. The effects of volcanic aerosols are illustrated in Figure 5, which shows the impact of the eruptions of El Chichón in 1982 and of Mt. Pinatubo in 1991 on the Version 7 TOMS minimum ocean reflectivity derived using the 380-nm channel with the final calibration developed below. The radiative transfer calculations used in the algorithm do not include aerosols, so the derived surface reflectivity is overestimated due to increased backscatter on these occasions.

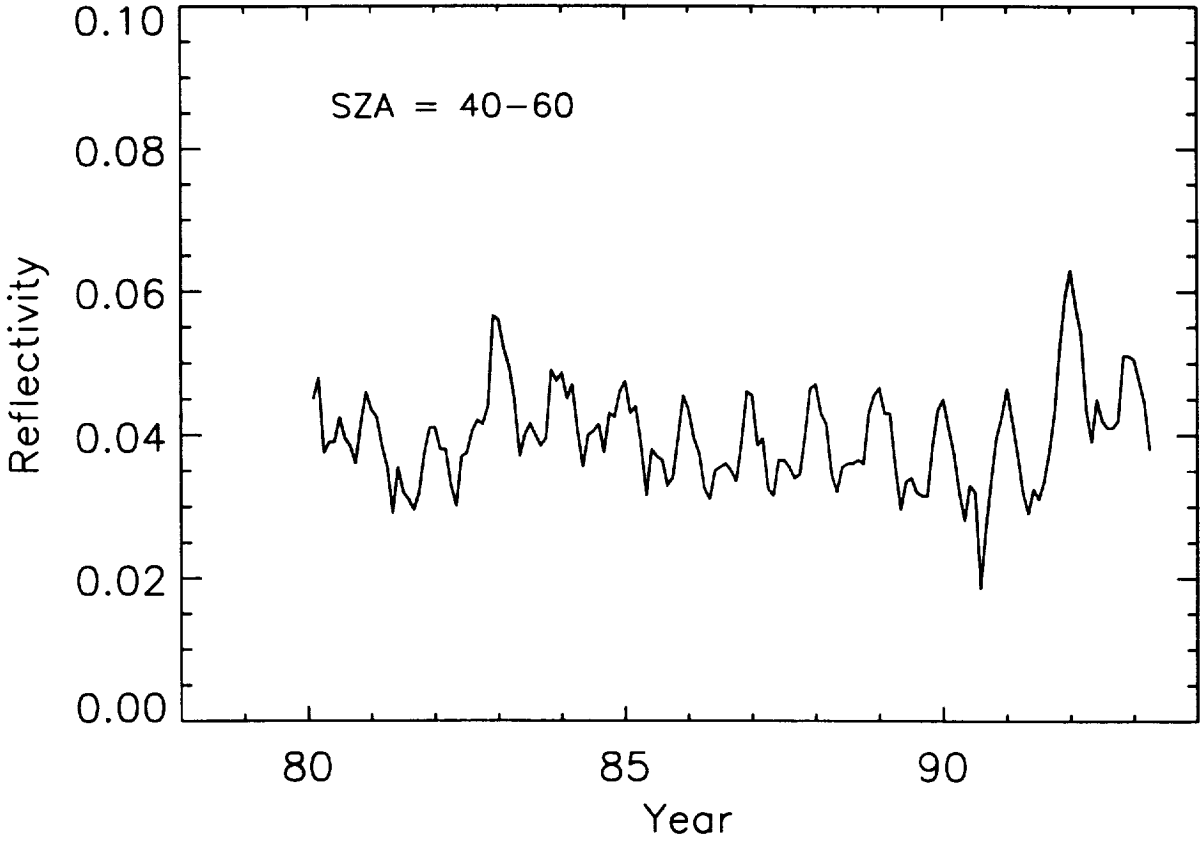

Figure 5. TOMS Version 7 monthly minimum surface reflectivity over the Pacific Ocean. This quantity is an estimate of the cloud-free ocean surface reflectivity as measured by TOMS.

A better method for determining the calibration drift, using the differential sensitivity to calibration error of a pair of reflectivity wavelengths, has been implemented for the Version 7 TOMS data. This approach is referred to as the spectral discrimination method. Given ε_i, which is the fractional calibration error (or instrument change) in the measured radiance at wavelength i, the difference in derived reflectivity for wavelengths i and j can be written to first order as,

$$R_i - R_j = k_i\varepsilon_i - k_j\varepsilon_j \tag{8}$$

where, $k=\Delta R/\Delta\varepsilon$ is the sensitivity of the derived reflectivity to an error in the measured Earth radiance. The sensitivity, k is a function of viewing geometry and surface reflectivity, and is calculated separately using the radiative transfer solution for each TOMS retrieval. This expression can be rewritten as,

$$R_i - R_j = k_i(\varepsilon_i - \varepsilon_j) + (k_i - k_j)\varepsilon_j \tag{9}$$

where the sources of drift in reflectivity between the two wavelengths are separated into a relative term and an absolute term. The first term on the right represents only the drift in the reflectivity measured by the i^{th} wavelength relative to the reflectivity derived from the j^{th} wavelength. The second term on the right represents additional drift between the two reflectivities resulting from an absolute calibration error in the j^{th} wavelength. The difference in sensitivities in this term is a consequence of Rayleigh scattering, which causes shorter wavelengths to be less sensitive to surface reflectivity changes than the longer wavelengths. This difference is particularly pronounced for low surface reflectivities where most of the backscatter ultraviolet radiation comes from the atmosphere rather than the surface. Under these conditions, a calibration error that is independent of wavelength can produce a wavelength dependent difference in derived reflectivity.

Figure 6 illustrates this behavior, showing $k(\lambda)$ for low reflectivity and high reflectivity cases separately. In the high reflectivity case, there is very little wavelength dependence in k, and the second term in Equation 9 is negligible. In this form, Equation 9 can be used effectively to derive the calibration error in wavelength i relative to wavelength j. In the low reflectivity case, given the error at i relative to j from the high reflectivity regime, the equation can be solved for the calibration error in wavelength j. Thus, the instrument changes can be derived directly from the uncorrected Earth radiances. To achieve good signal to noise for deriving the absolute calibration error using the second term, the two extreme reflectivity wavelengths of TOMS are used. Since the value of k_{331}-k_{380} is roughly 0.3 at low reflectivities, one needs to measure R_{331}-R_{380} to an accuracy of 0.003 to derive absolute calibration to 1 percent. The relative calibration differences are determined to higher precision using data from the high reflectivity cases where k is relatively large.

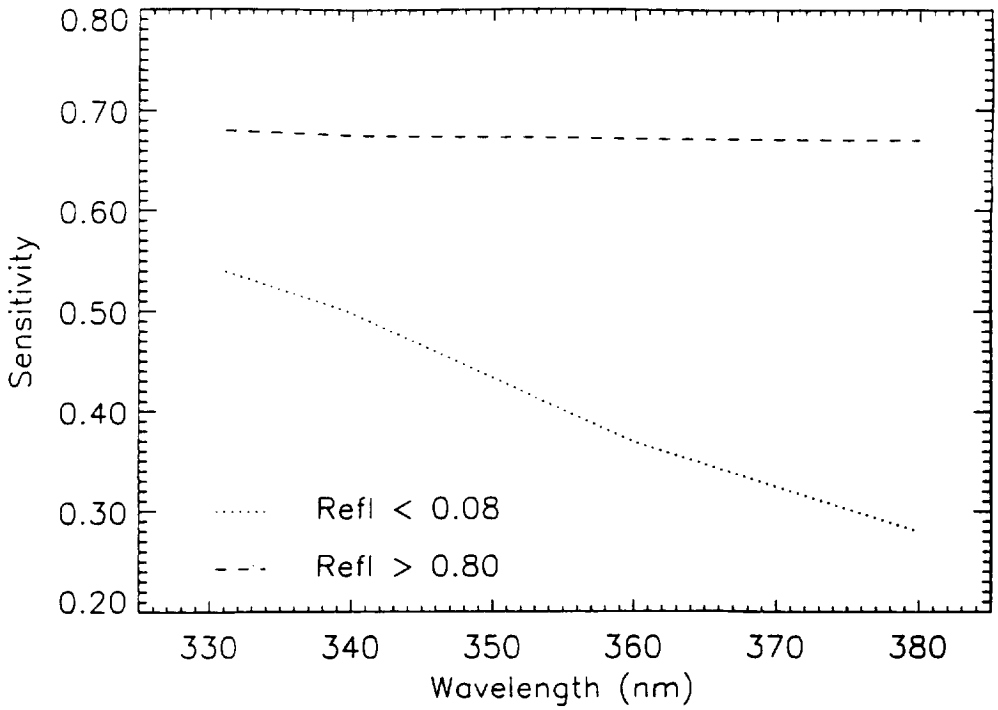

Figure 6. Algorithmic sensitivity of the surface reflectivity measurement at the longer TOMS wavelengths for low and high reflectivity cases. Rayleigh scattering over a low reflectivity surface causes a wavelength dependence in reflectivity algorithm sensitivity.

Figure 7 shows the reflectivity difference, R_{331}-R_{380}, as a function of time for low and high reflectivities derived using the uncorrected TOMS radiances, normalized using the initial solar measurement. The curves are different in the different reflectivity regimes, indicating both drift at 331 nm relative to 380 nm (high reflectivity), and drift in absolute calibration 380 nm (low reflectivity). The solid curves are smooth fits to the data. The standard deviations of the data about the fits are 0.0026 and 0.0028 for the high and low reflectivity regimes, respectively. Thus, estimates of the TOMS instrument change can be computed to accuracies of better than 1 percent. The impact of non-synchronization of the TOMS chopper wheel described in Section 7 was removed from the TOMS radiances in this analysis to allow for determination of "smooth" changes in the instrument throughput.

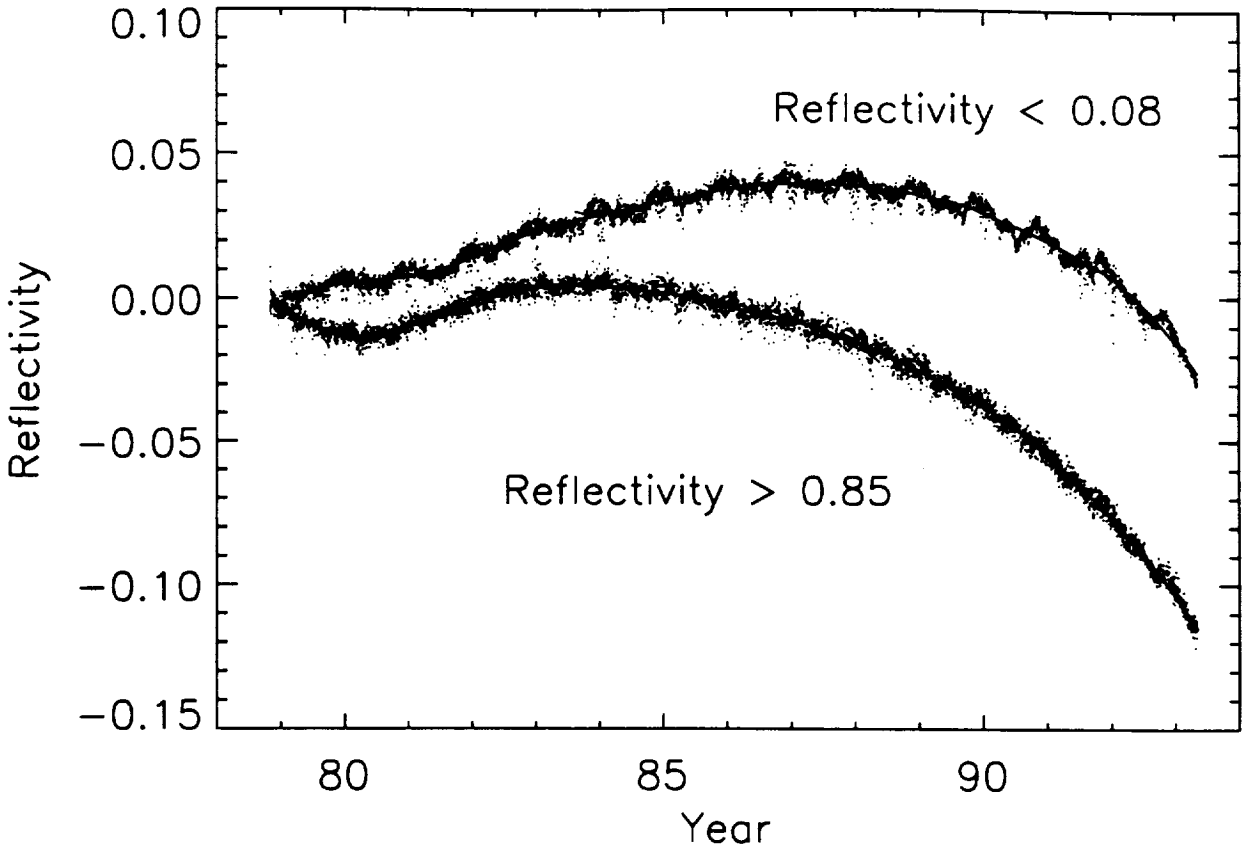

Figure 7. Observed difference between surface reflectivity derived from the 331-nm and 380-nm channels of TOMS using uncorrected radiance measurements. Different responses in different surface reflectivity regimes indicate the presence of a time-dependent absolute calibration error in 380-nm channel. The high reflectivity case indicates the wavelength dependent calibration error of the 331-nm channel relative to the 380-nm channel.

3.3 Quadratic Fit for Ozone Wavelengths

In order to calibrate the shorter ozone wavelength channels of TOMS, a simple quadratic fit in wavelength to the calibration results at the longer reflectivity wavelengths has been used. In previous studies [*Herman et al., 1991*], the PJM has been used to characterize the wavelength dependent calibration error at the shorter ozone wavelengths (312 and 317 nm). For TOMS, a critical step in the PJM is the assumed form of the wavelength dependence of the calibration error. In Version 6, the form for the diffuser plate degradation was determined using SBUV PJM results. These results were based on the D-pair wavelengths (306 and 313 nm) which are far less sensitive to errors in the assumed wavelength dependence than any of the TOMS pairs. In the interest of clarity, and more importantly, to establish independence between the TOMS and SBUV data sets, we have used the more explicit approach of assuming a quadratic form in Version 7 for the wavelength dependence of the calibration error. This is accomplished using a quadratic fit in wavelength to the smoothed instrument changes already derived for the longer reflectivity

wavelengths. The quadratic is applied to the individual sets of daily estimates of instrument change at the 380, 360, and 331 nm channels, and extrapolated to the shorter ozone sensitive wavelengths. The 340-nm channel is not used because it is more strongly affected by the "toggling" errors discussed in Section 7.2. As discussed in Section 2.2, the exact form assumed for this wavelength dependence is important in terms of its impact on derived ozone. We will discuss the potential systematic error associated with this assumption in Section 3.4, and check the results of the quadratic fit using the PJM.

The results of the spectral discrimination analysis and the quadratic fit are summarized in Figure 8. This estimate of the TOMS instrument change is used in the Version 7 reprocessing to calibrate the measured radiances. These calibrated radiances are normalized by initial measurements of solar flux as described above to form the I/F values used to derive ozone. Note that the toggling impact estimate discussed below in Section 7.2 has been put back into the final result to provide a complete estimate of the instrument change. Also shown in Figure 8 is the implied diffuser degradation which is simply the ratio of the total change (Figure 3) to the derived instrument change. These results will be discussed further below in the following two subsections.

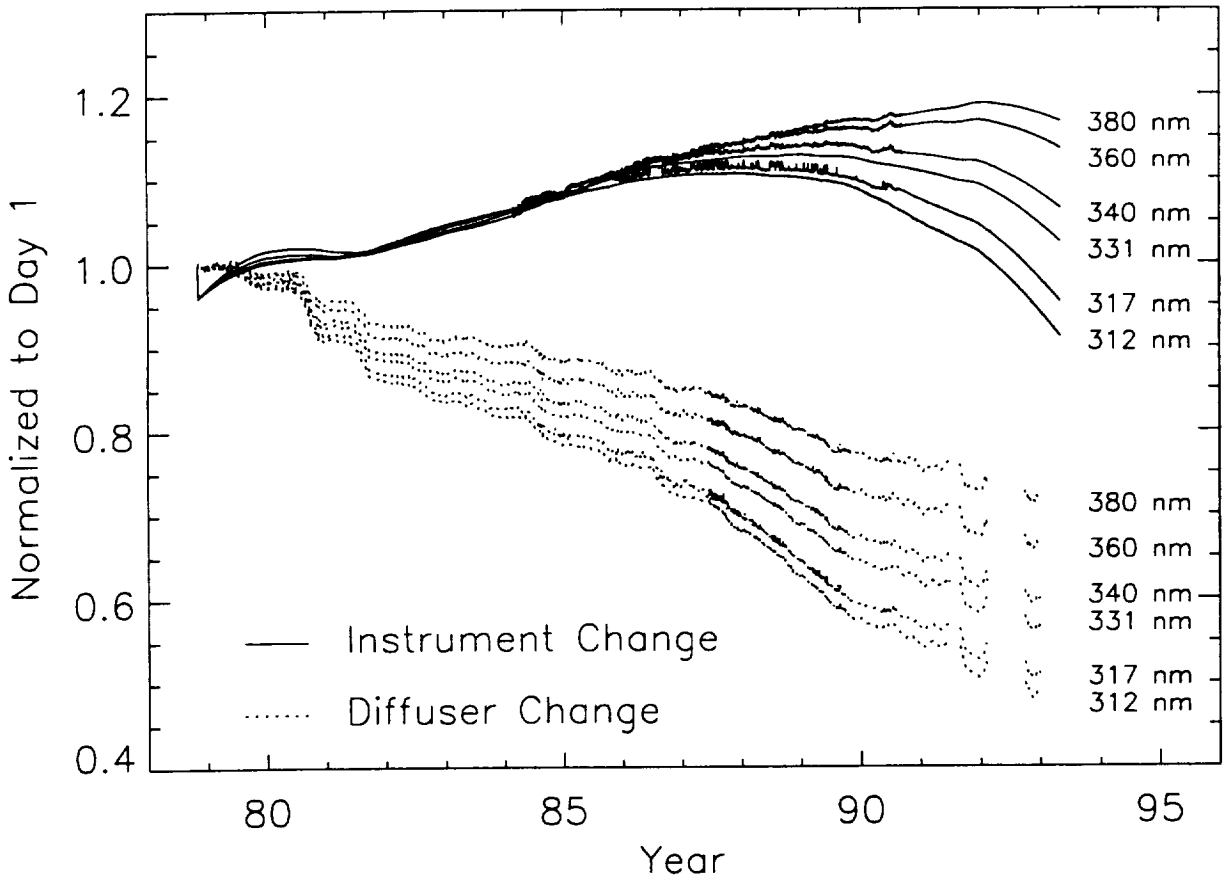

Figure 8. Diffuser and instrument components of the total change exhibited in TOMS "raw" solar flux (Figure 3) as derived using the radiance calibration methods described.

3.4 Error Analysis

The argument presented above near the end of Section 3.2 relating statistical noise in fitting (R_{331}-R_{380}) reflectivity differences to the uncertainty in the precision of the instrument change estimates at the longer reflectivity wavelengths can be extended to the shorter ozone wavelengths by using the uncertainties in the longer wavelengths to drive a perturbation analysis of the quadratic fit results. This analysis gives precision estimates of less than 0.005 in reflectivity for the longer channels, and of about 1.5 percent in ozone for the shorter channels at the 95 percent confidence level. With this type of precision, the trends in ozone could be determined to high accuracy. However, this

simple approach does not account for systematic error sources that are present in the data. The assumption of a quadratic form to characterize the wavelength dependence of the TOMS instrument change is the most obvious potential source of systematic error, and is discussed below. Another potential systematic error has to do with the combination of possible angular dependent errors in the derived surface reflectivities and the drifting orbit of the Nimbus–7 spacecraft.

The drift in the orbit of the Nimbus–7 spacecraft away from a local noon equator crossing time results in generally larger solar zenith angles associated with TOMS measurements toward the end of the data record. To minimize this potential systematic error source, we have used near-nadir data from TOMS for a fixed solar zenith angle range for both the low and high reflectivity cases. We have also restricted the low reflectivity case to data from the Pacific Ocean to reduce any effects due to inhomogeneities in surface reflectance. Since spectral discrimination uses differential reflectivity sensitivities at the longer TOMS channels, it is much less affected by the presence of volcanic aerosols than earlier stabilization methods. None of the volcanic effects seen clearly in the ocean reflectivity minima of Figure 5 are visible at all in the reflectivity differences shown in Figure 7. In spite of the robust nature of the spectral discrimination technique, small systematic errors associated with the orbital drift of the Nimbus–7 satellite cannot be ruled out.

To help assess the possible impact of such errors, we have estimated the TOMS instrument change in the 331-nm channel relative to 380 nm based on the reflectivity differences from three different populations. As shown in Table 1, these populations are distinguished by solar zenith angle range and the criterion defining the high reflectivity case. Each of these populations is considered viable, though the case we used (first line in Table 1) is considered optimal. The range of values for total instrument change is 0.6 percent. This level of uncertainty propagates through perturbation of the quadratic fit to an uncertainty of approximately 1.5 percent in total ozone at the end of the data record or about 1.0 percent/decade.

Table 1. Spectral Discrimination Results Based on Alternate Populations

Population Description		Relative Drift at 331 nm (%)
Solar Zenith Angle (Degrees)	Reflectivity Limits	
20–35	>0.85	–0.2
20–35	0.70–0.85	0.1
50–65	>0.80	0.4

As mentioned previously, the assumption of quadratic wavelength dependence in the instrument change is a likely source of systematic error in the Version 7 calibration technique. The quadratic form can be tested by predicting TOMS solar flux measurements at the ozone wavelengths based on a fit to the long wavelengths (Figure 9). We note, however, that the TOMS solar flux is affected by both instrument and diffuser changes. The instrument change over the first five years is very nearly independent of wavelength, while the diffuser degradation has a strong wavelength dependence from the beginning of the data record. By the end of the record however, both the instrument and diffuser components show strong wavelength dependence. The results in Figure 9 indicate that the quadratic form fits both components fairly well, and is good to about 1 percent. This error appears systematic at the end of the record, though some of the variability may be due to errors in the correction for the BRDF of the solar diffuser at high solar azimuth angles.

Another approach to checking the assumed quadratic wavelength dependence at the shorter ozone channels is to use the pair justification method [*Herman et al., 1991*]. The correct calibration will result in consistent ozone values derived using different pairs of wavelengths. The fundamental equations for the pair justification technique are,

$$\Omega_i = \Omega_{true} + \varepsilon_i S_i \tag{10}$$

$$\Omega_j = \Omega_{true} + \varepsilon_j S_j \tag{11}$$

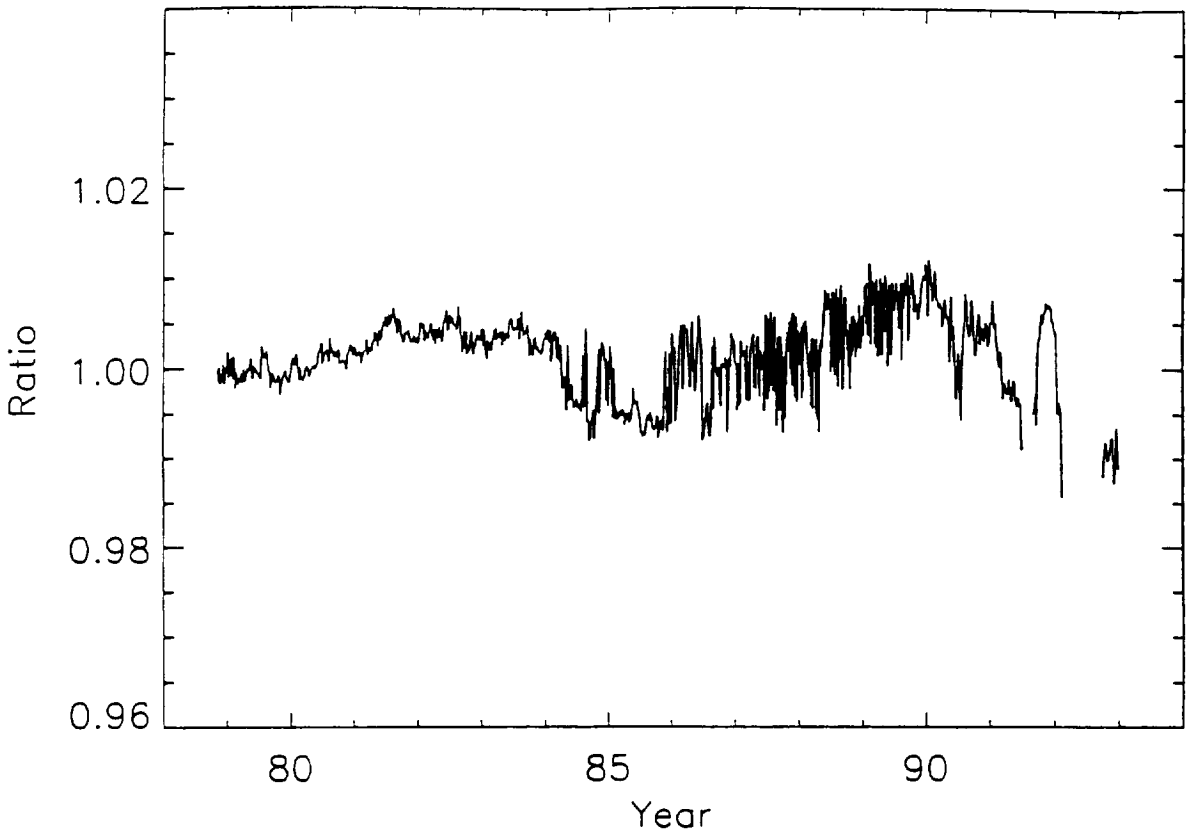

Figure 9. Ratio of TOMS solar flux at 312-nm predicted using a quadratic fit to 380-nm, 360-nm, and 331-nm solar fluxes to the measured 312-nm solar flux. The ratio indicates the possibility of systematic errors no greater than about 1 percent. This error is approximately equivalent to 1 percent in total ozone.

and,

$$f_{ij} = \frac{\varepsilon_i}{\varepsilon_j} = \frac{\delta\lambda_i}{\delta\lambda_j} \tag{12}$$

where,

Ω_i = the measured ozone change at wavelength pair i
Ω_{true} = the true ozone change
ε_i = the calibration error at wavelength pair i
S_i = the pair sensitivity to calibration error
f_{ij} = the ratio of calibration errors at wavelength pair i and j
$\Delta\lambda_i$ = the wavelength separation of pair i.

Equations 10 and 11 express the fact that different wavelength pairs that are properly calibrated measure the same true ozone change. For pair justification, the A-pair (331 nm–312 nm) and B'-pair (331 nm–317 nm) are used because of their relatively large difference in sensitivity to wavelength dependent calibration errors, and the broad range of viewing conditions over which they provide effective retrieval characteristics. Equations 10 and 11 form a system with three unknowns, and a third equation is required to provide a solution. Equation 12 represents the first order assumption of a linear wavelength dependence in any residual calibration error. This assumption is motivated by the fact that a quadratic fit has been used to remove the second order dependence, and that the residual error is small as shown in Figure 9. The three equations can be combined to yield,

where,

$\delta\Omega_j$ = the error in ozone measured by pair j (Ω_j - Ω_{true})

S_{ij} = the ratio of pair sensitivities to calibration error (S_i/S_j)

$$\delta\Omega_j = \frac{(\Omega_i - \Omega_j)}{(f_{ij}S_{ij} - 1)} \tag{13}$$

Figure 10 shows the A-pair ozone error ($\delta\Omega_j$), derived using Equation 13 and the B'-pair and A-pair ozone values obtained using the Version 7 instrument characterization shown in Figure 8. This result indicates a systematic trend error of about 1 percent in ozone over the entire data record. No correction has been made based on these results, because this error is smaller than the statistical uncertainty developed above. Also, if the residual error is nearly linear with wavelength, the resulting error in ozone trends derived using the Version 7 triplet formulation will be very small as discussed in Section 2.2.

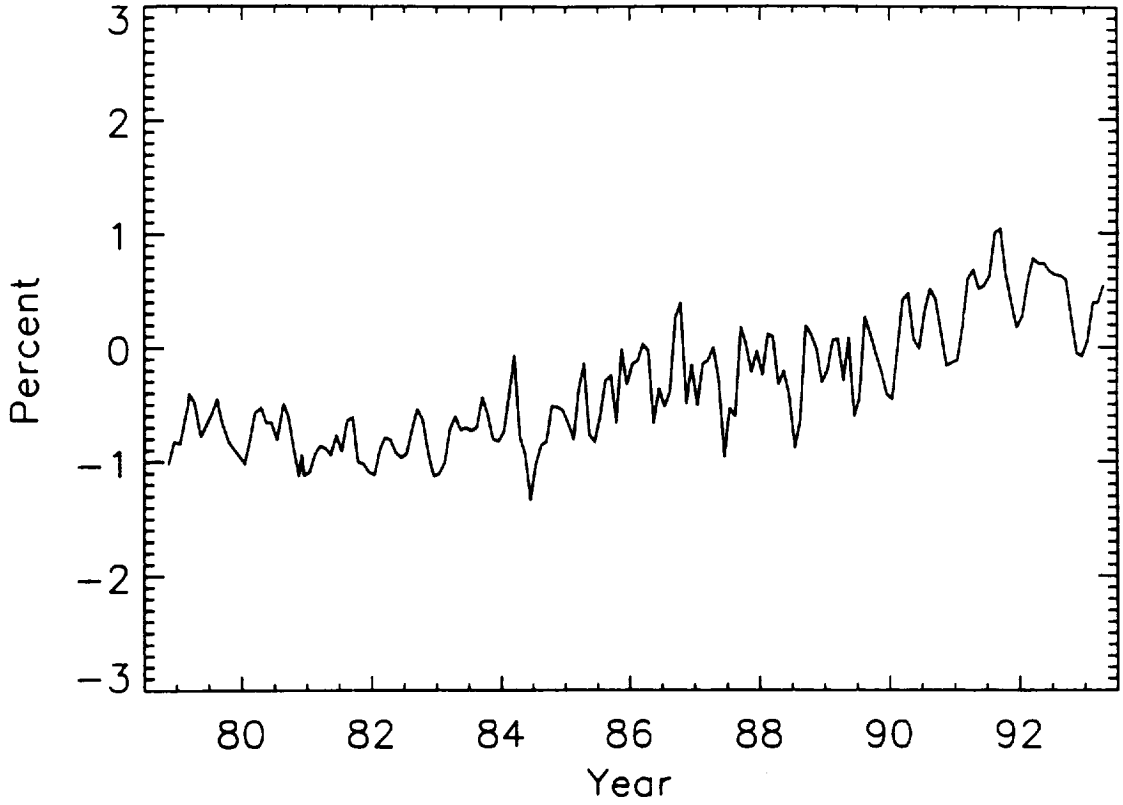

Figure 10. Long-term drift in TOMS A-pair ozone as determined using the PJM with a first order assumption for the wavelength dependence of the calibration error. The triplet formulation used in the Version 7 algorithm is much less sensitive to this error than the Version 6 A-pair (Section 2.2).

3.5 Validation

Figure 8 shows the instrument change at 380 nm derived using Equation 7, the instrument change at the other reflectivity wavelengths derived relative to 380 nm, and the results of the quadratic fit for the ozone wavelengths. These results are roughly consistent with the TOMS uncorrected equatorial Earth radiances shown in Figure 4. Also shown in Figure 8 is the diffuser degradation implied by the derived instrument changes. These changes are monotonic except when goniometric errors occur near the end of the data record, and exhibit increased rates of degradation during periods of accelerated diffuser deployments as expected. Figure 11 shows the implied diffuser degradation as a function of the solar exposure time of the diffuser plate for Version 7, as well as the previous Version 6. The Version 6 calibration was extrapolated from October 1989 (about 1,100 hours) based on continuing solar

measurements and the assumption that subsequent diffuser degradation would be linear in exposure time. The results in Figure 11 suggest some second order dependence in the diffuser degradation. Figure 11 also indicates an error in summer 1990 (1,120 hours) resulting from goniometric errors in the measurement of solar flux. This second error is wavelength independent and though it leads to an error in the TOMS reflectivity of about 0.03, it had very little effect on the Version 6 TOMS ozone. Overall, the Version 6 and Version 7 results compare quite well for the period before 1990. Considering that they are the results of independent techniques, we consider the agreement to be quite compelling.

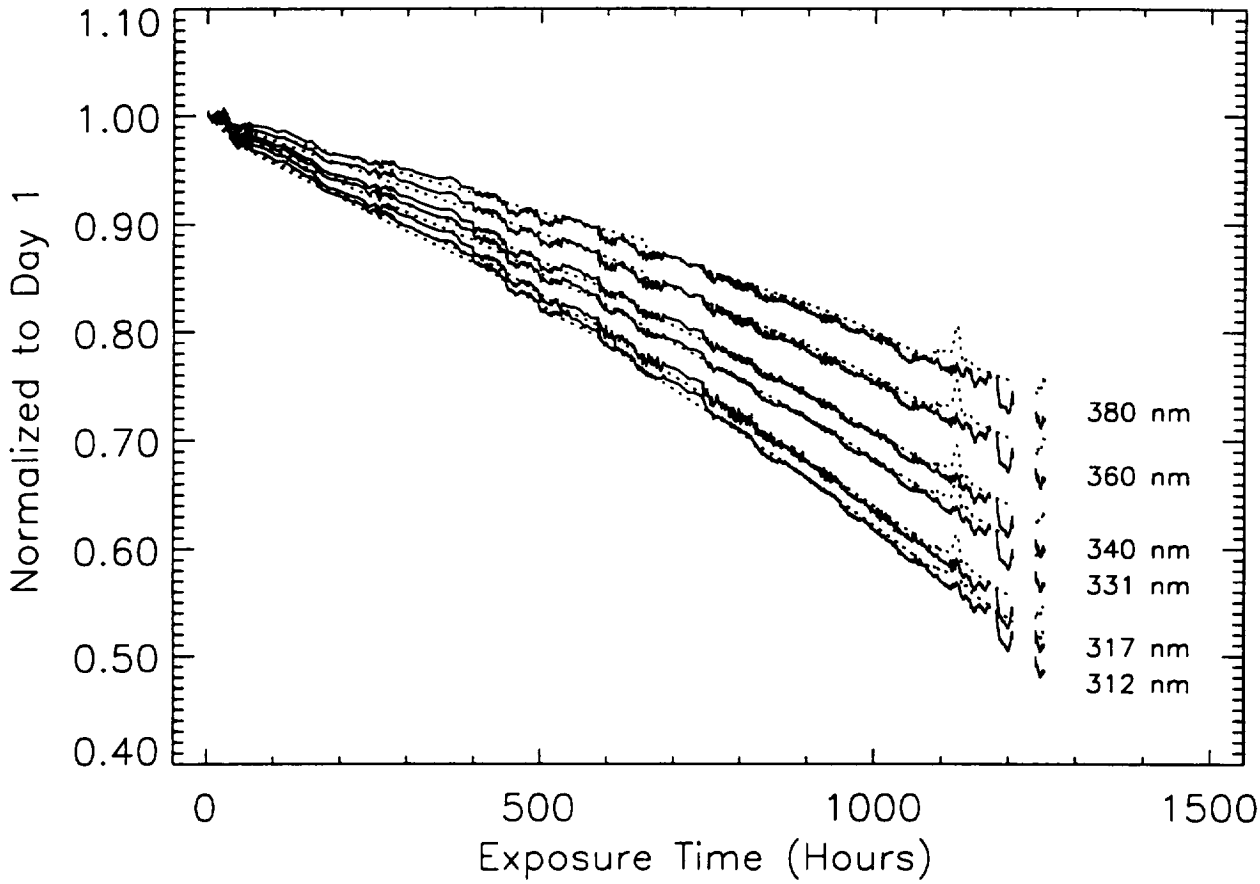

Figure 11. Implied diffuser degradation as a function of solar exposure time. Version 7 results (solid) are compared with the previous Version 6 (dotted).

An analysis of Nimbus–7 TOMS ice radiances similar to a previously reported study of Meteor-3 TOMS [*Jaross et al., 1995*] has been carried out as a validation of the spectral discrimination result for the 380-nm channel. In this study, the highly reflective surfaces of Greenland and Antarctica are assumed constant and used as a reference source in monitoring the TOMS instrument changes. The raw TOMS counts measured at nadir are regressed against solar zenith angle so that the effects of solar zenith angle dependence can be removed before comparison is made to a reference year. The results of this study, shown in Figure 12, agree to within about 2 percent in measured radiance or to better than 0.01 in derived surface reflectivity. The statistical error bars shown in Figure 12 are quite small, but the estimated overall uncertainty of the ice radiance technique is about 1 percent.

To summarize, the TOMS Instrument changes estimated using the spectral discrimination method in conjunction with the quadratic fit are accurate to within 1 percent/decade. They provide a self-consistent picture of reasonable instrument changes along with plausible diffuser degradation, and they provide stable reflectivity over the long-term for ice covered regions and open ocean. Some further validation is provided in Section 9.2. Some further aspects of the TOMS instrument behavior are discussed in the following sections. Some of this work is motivated by or based on comparison of radiances measured by TOMS and SBUV.

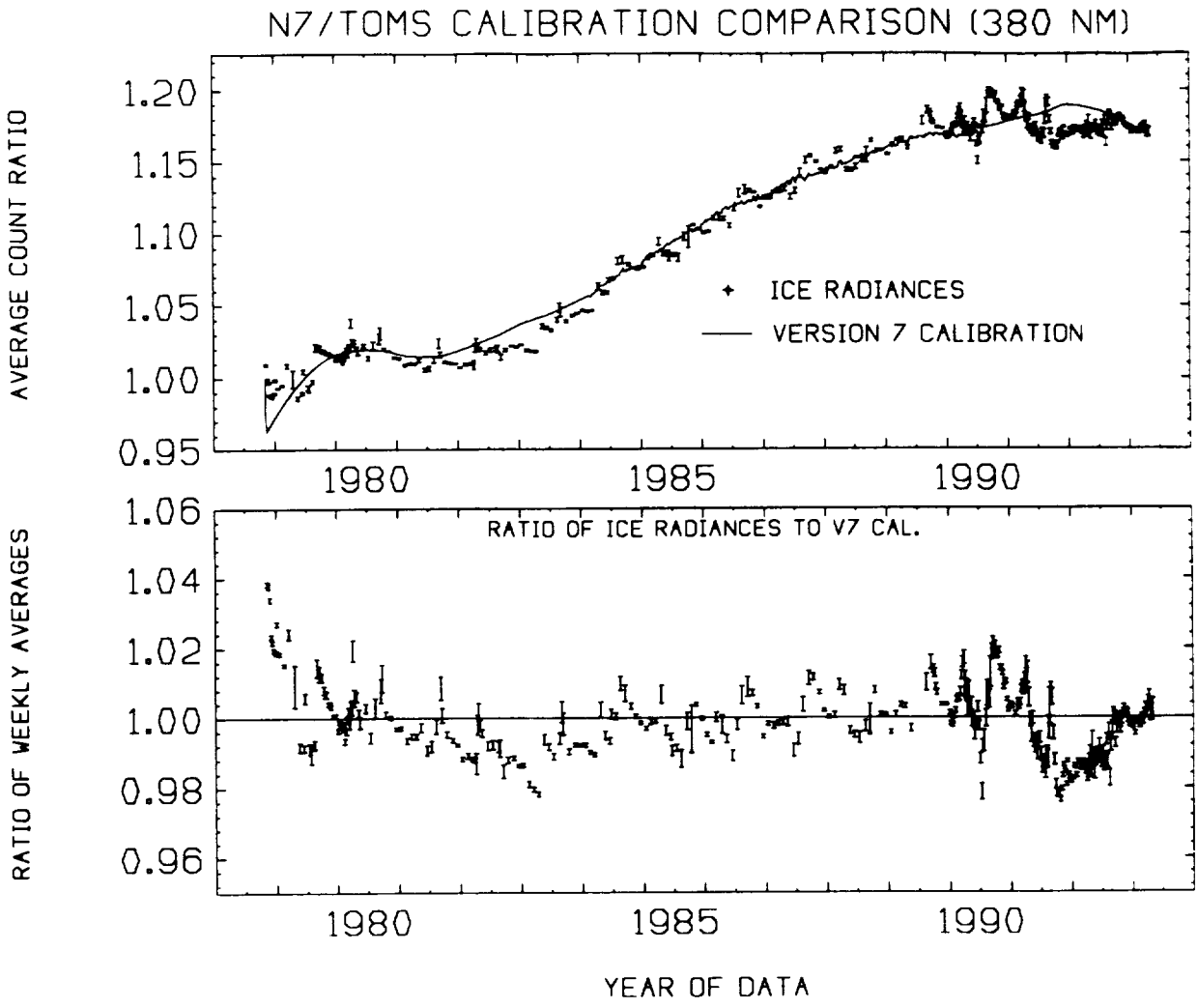

Figure 12. Comparison of spectral discrimination results at 380 nm and ice radiance calibration technique. Results agree to 2 percent in radiance or 1 percent in derived reflectivity.

4.0 TOMS–SBUV COMPARISONS

4.1 Comparison Method

The TOMS is a scanning instrument with a 49 km of instantaneous field of view (IFOV). The SBUV, also on board Nimbus–7 is a nadir looking instrument with a 188 km of IFOV. While the TOMS wavelength sampling is interleaved to avoid scene differences between wavelengths, the SBUV samples wavelengths sequentially [*Heath et al., 1975*]. SBUV measures at a shorter complement of wavelengths used to derive the upper level vertical distribution of ozone, but also measures four wavelengths at 313, 318, 331, and 340 nm that are very near the TOMS wavelengths. The TOMS and SBUV are co-aligned so that the larger SBUV IFOV can be emulated using an area weighted average of TOMS measured radiances (Figure 13). The weighting is wavelength dependent to account for the motion of the SBUV IFOV between measurements at adjacent wavelengths. The motion of the SBUV IFOV during the measurement at a given wavelength is not taken into account and contributes to error in the comparison. The degree of coincidence achieved by this technique is validated by varying the interpolation and area weighting factors to simulate displacements in the TOMS composite IFOV. The minimum variance in the TOMS–SBUV radiance difference is found at the expected SBUV IFOV locations for the four wavelengths of interest to within a few kilometers.

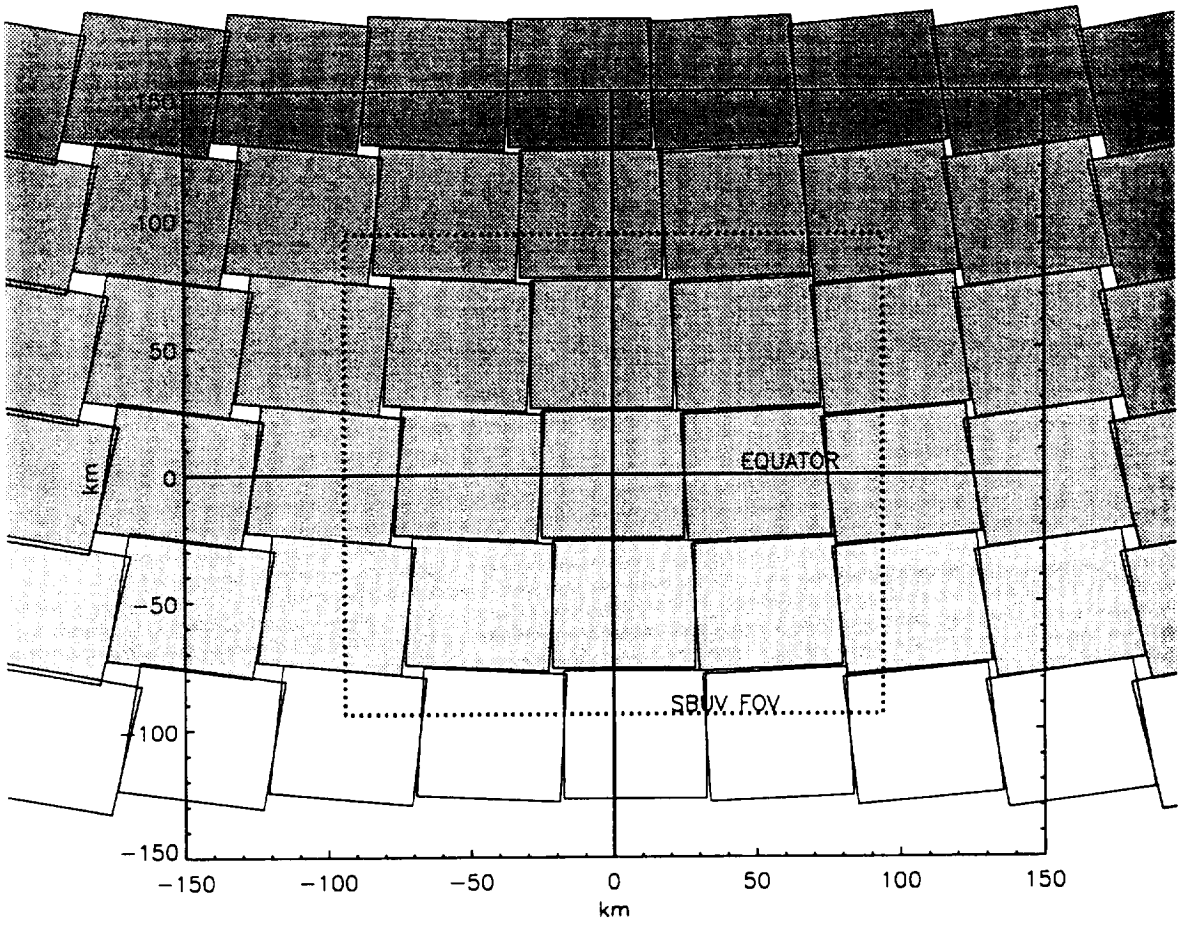

Figure 13. Sample overlay of TOMS near-nadir IFOV and the larger SBUV IFOV for a single wavelength.

The TOMS–SBUV radiance difference must be adjusted to account for small differences in the actual wavelengths measured by each instrument. The TOMS and SBUV instruments measure somewhat different wavelengths initially, and the SBUV wavelengths are known to drift with time due to mechanical wear in the wavelength selection cam [*Fleig et al., 1990*]. These differences are all taken into account using ratios of radiative transfer calculations at the

two different wavelengths (impact ratio). The same radiative transfer solution used in the TOMS algorithm [*McPeters et al., 1996*] is used to calculate the impact ratios. The changes in SBUV wavelength with time are of the order of 0.05 nm. They are taken into account using the impact ratio calculated for 0.05 nm scaled by the actual wavelength separation at a given time. Figure 14 shows the results of this type of comparison between SBUV and the previous Version 6 TOMS for March 19, 1980. The data exhibit a bias with an unusual latitude dependence.

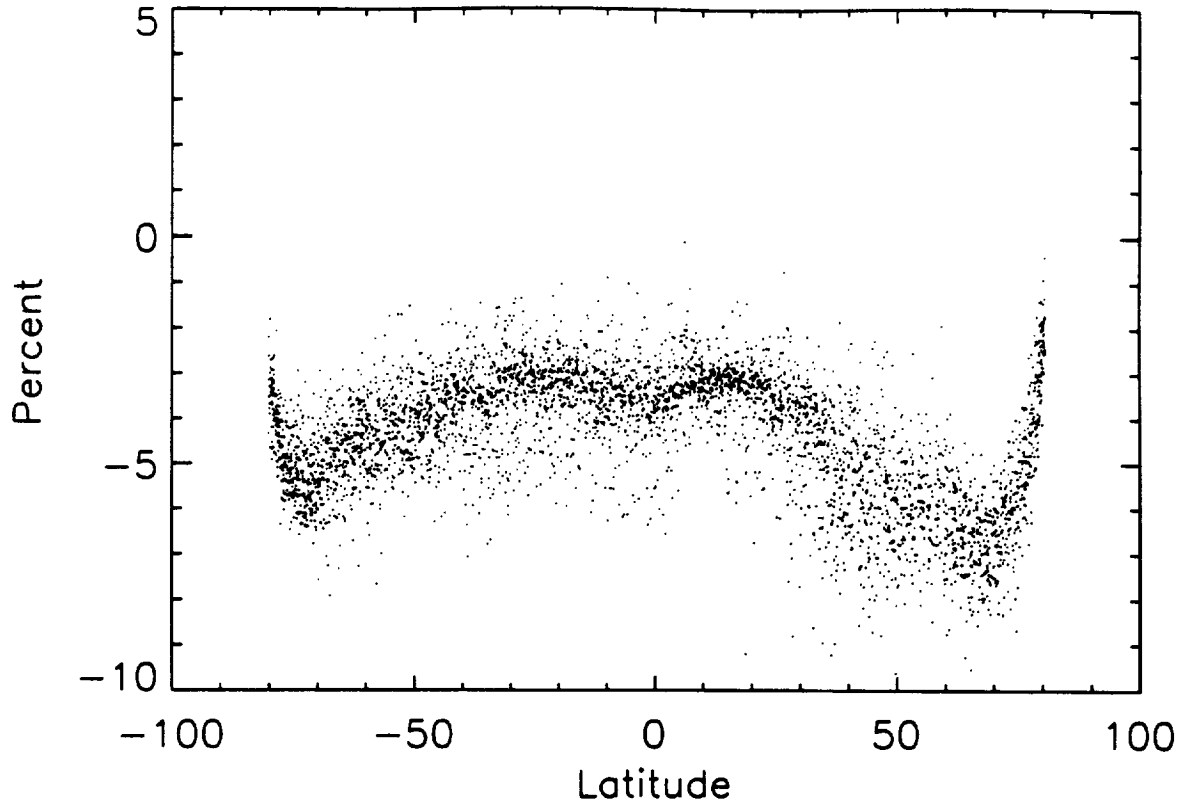

Figure 14. Uncorrected TOMS–SBUV percent difference in A-pair radiances for individual coincidences on March 19, 1980. One percent decrease in A-pair radiance is roughly equivalent to one percent increase in derived total ozone.

4.2 Definition of N-value

In the calculation of ozone, the measured earth radiances are normalized by the measured solar flux. It is the logarithm of the normalized Earth radiance, however, that is more nearly proportional to the total column ozone and linearizes the table look-up procedure used in the ozone algorithm. A convenient quantity used to facilitate this parameterization is the N-value,

$$N = -\ 100\ Log_{10}(I/F) \tag{14}$$

where I is the measured Earth radiance and F is the measured solar irradiance. The N-value is used in some of the discussion of TOMS–SBUV comparison results presented below where logarithmic representations of the radiances are convenient.

4.3 A Variant of the Langley Method

The differences shown in Figure 14 may be the result of relative radiometric calibration error, relative wavelength calibration error or some combination of the two. These error sources can be separated using a variation of the Langley method used in the calibration of Dobson instruments [*Komhyr et al., 1989*]. The difference in normalized radiance between the two instruments (expressed in N-value) can be written as:

$$\Delta N_{meas} = \Delta N_{calib} + \Delta\alpha \partial N / \partial\alpha \quad (15)$$

where:

ΔN_{meas} = the measured TOMS–SBUV N-value difference
ΔN_{calib} = the TOMS–SBUV radiometric calibration offset
$\Delta\alpha$ = the difference in absorption coefficient due to wavelength difference
$\partial N/\partial\alpha$ = the sensitivity of theoretical N-value to $\Delta\alpha$.

This equation defines a line of slope $\Delta\alpha$ and y-intercept ΔN_{calib}. The technique is similar to the Langley method in that the sensitivity is a function of slant path, so a regression of data taken at a range of slant paths can be used to separate the sources of calibration error. A sample regression for the 313-nm measurements near the vernal equinox of 1980 is illustrated in Figure 15. These results indicate that the TOMS radiometric calibration is about 3.5 percent too high, and that the wavelength calibration is 0.19 nm too long, assuming that the SBUV is correctly calibrated. These considerations motivated a reanalysis of the original TOMS wavelength calibration procedure discussed in Section 5, and an adjustment of the initial TOMS calibration discussed in Section 6.

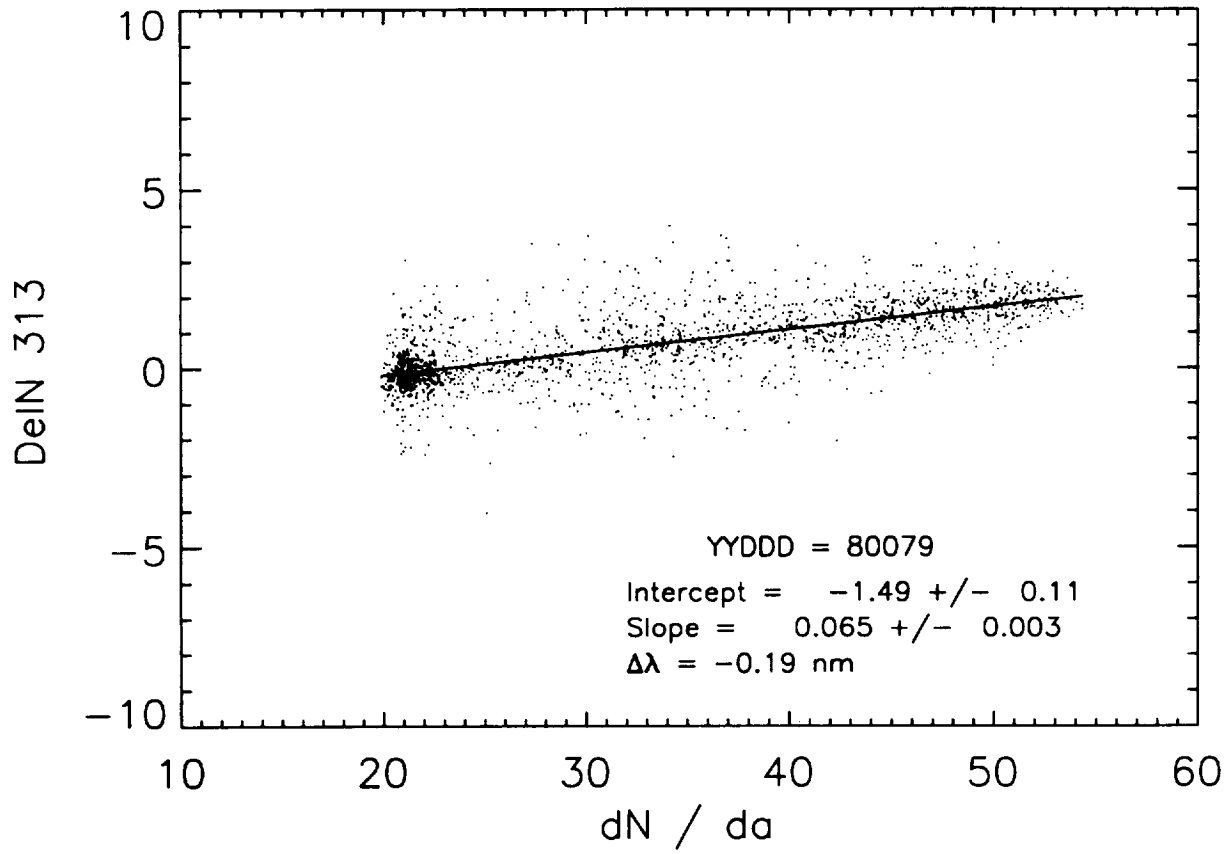

Figure 15. Separation of relative calibration error sources by regression of TOMS–SBUV normalized radiance differences as a function of sensitivity to wavelength calibration error. The y-intercept is an estimate of the radiometric calibration offset, and the slope is an estimate of the error in absorption coefficient associated with wavelength calibration errors.

5.0 TOMS WAVELENGTH SCALE ADJUSTMENTS

5.1 Background

It has long been noted that a shortward shift in the TOMS wavelength scale would tend to explain the initial bias between Nimbus–7 TOMS and SBUV. Also, the analysis presented above in Section 4 indicates that the unusual latitude dependent bias at the A-pair wavelengths can be explained by a wavelength difference of about 0.2 nm (Figures 14 and 15). These considerations motivated a re-analysis of the original TOMS wavelength calibration procedure.

5.2 Analysis Method and Results

Two main error sources exist in the original TOMS prelaunch wavelength calibration. The larger source results from a misinterpretation of wavelength calibration monitoring data taken previous to the launch of the instrument. The smaller source results from uncertainty in the original wavelength calibration procedure [*Hughes STX, 1994*].

First, consider the original wavelength calibration procedure. The TOMS instrument has a single, fixed monochromator with exit slits designed to select the measured wavelengths. To determine the prelaunch calibration, a mercury source was placed at the TOMS entrance aperture to produce images of the diffracted emission lines on a film strip. Images of the exit slits were superimposed on the film strip by placing a white light source near the exit slits. This provides measurements of the slit widths, as well as the relative positions of the lines of mercury and the exit slits (Figure 16). Determination of the TOMS wavelengths and bandpass involves interpolating and extrapolating from the known wavelengths of the mercury lines to the positions of the exit slits on the film strip. A second order regression (very nearly linear) was performed on these data, scaling physical position on the film strip to wavelength.

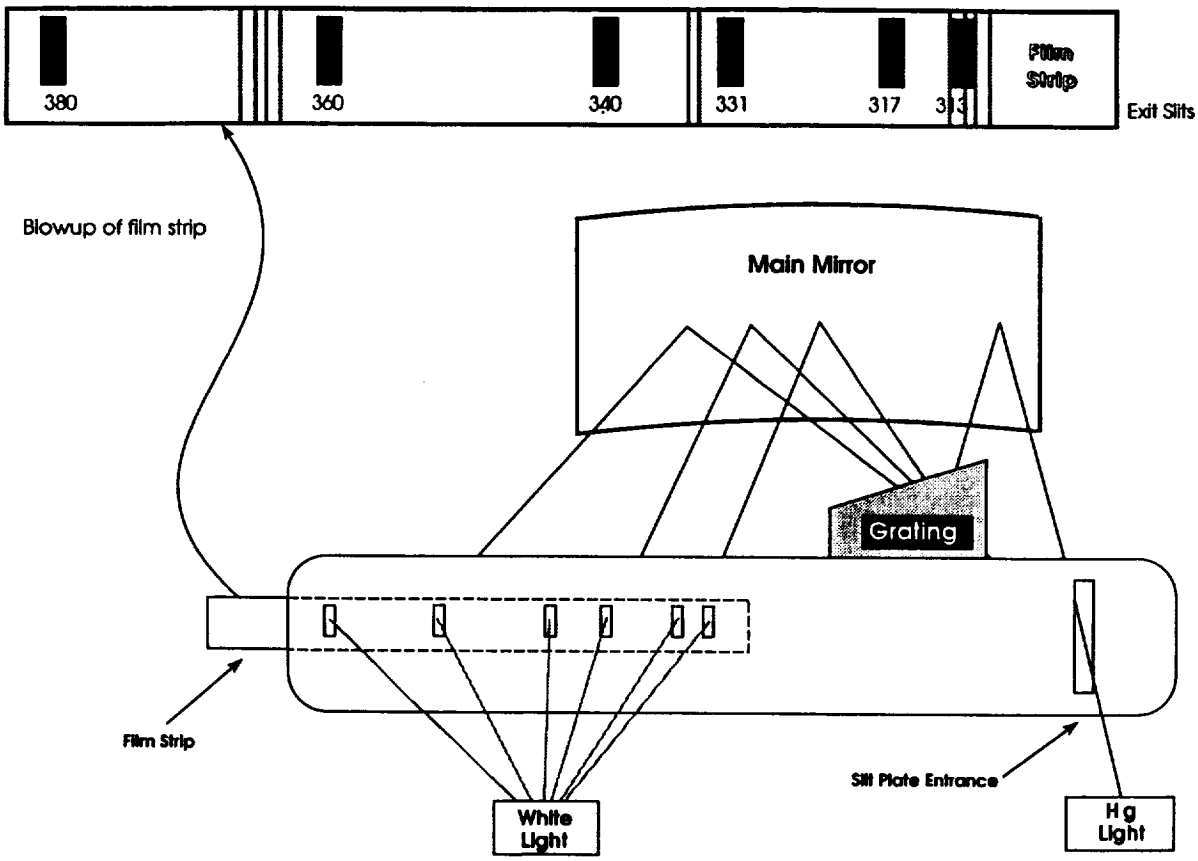

Figure 16. Schematic of TOMS wavelength calibration procedure. Images of the exit slits are used to locate TOMS wavelengths relative to the known wavelengths of the mercury lines.

This analysis was performed in 1978 for the Nimbus–7 TOMS flight model as well as the engineering model which was subsequently recalibrated and flown on the Russian Meteor-3 spacecraft [*Jaross et al., 1995*]. The additional information acquired from the engineering model proved useful in reanalyzing the wavelength calibration data. Comparisons of the exit slit widths measured for the engineering model in 1979 and 1990 and those measured for the Nimbus–7 TOMS indicate no inconsistencies. However, comparisons of the mercury line widths indicate that three of the line widths measured from the Nimbus–7 TOMS filmstrip were probably in error. This conclusion is confirmed using linear dispersion modeling of the mercury line locations [*Hughes STX, 1994*]. An error in the line width implies that the line center is mislocated. The assumption is made that for each of these lines, one edge was measured correctly and one incorrectly. By repeating separate regressions of line positions determined using alternate edges of each of the errant lines, the correct edge and the incorrect edge are successfully identified in two of the three cases through an analysis of the fit residuals (Table 2). Fortunately, the third line is in a redundant location and can be discarded without degrading the calibration method. In conjunction with the line widths from the engineering model, the good edges are used to locate the line centers. The residuals of the regression to the corrected line centers are reduced by a factor of 10 over the original analysis. In this way, small errors in the Nimbus–7 TOMS wavelength calibration of the order of 0.05 nm are identified.

Table 2. Standard Deviations of Wavelength Scaling Regressions Based on Various Combinations of Assumptions About the Positions of the Mercury lines at 312 nm and 334 nm

Line Location Assumed	Use 312-nm Long Edge	Use 312-nm Short Edge	Use 312-nm Original Center
Use 334-nm Long Edge	0.04970	0.00005	0.01288
Use 334-nm Short Edge	0.05410	0.00025	0.01492
Use 334-nm Original Center	0.05187	0.00013	0.01387

The larger source of error in the TOMS wavelength calibration was a result of misinterpretation of calibration monitor data. After the prelaunch wavelength calibration was performed, the relative stability was monitored during preflight testing using the TOMS internal wavelength calibration monitoring system [*Heath et al., 1978*]. These data indicated that a shift of +0.058 nm occurred prior to launch in November 1978. A careful reassessment of these data, however, indicates a sign error in the determination of this shift. This apparently resulted from confusion about the order in which the wavelengths are measured during the wavelength calibration monitoring sequence. The instrument contractor identified this error at the time, but for some unknown reason, a correction was not implemented. This means that an adjustment of -0.116 nm (2 x -0.058 nm) must be made to the published TOMS wavelengths [*McPeters et al., 1993*] in addition to the small errors determined by re-analysis of the film strip data. The total adjustment to the original wavelength calibration that has been applied in the Version 7 data is summarized in Table 3. We estimate that the error in the overall wavelength calibration procedure is less than 0.1 nm.

Table 3. Summary of TOMS Wavelength Calibration Adjustments

Revised Nimbus–7 TOMS Wavelength Scale [recommended]			
Nominal Wavelength [*nm*]	Version 6 Value [*nm*]	Recommended Change [*nm*]	Version 7 Value [*nm*]
312.5	312.51	–0.17	312.34
317.5	317.51	–0.16	317.35
331.2	331.25	–0.19	331.06
339.8	339.86	–0.20	339.66
360.0	359.96	–0.08	359.88
380.0	380.01	–0.06	379.95

5.3 Validation

These wavelength calibration adjustments bring the TOMS into much better agreement with SBUV. The impact of the wavelength adjustments on the TOMS–SBUV A-pair radiance comparisons is illustrated by Figure 17 which shows that the latitude behavior seen in Figure 14 is removed when the TOMS wavelength scale adjustment is taken into account. Figure 18 illustrates the impact of the TOMS wavelength scale adjustment on TOMS–SBUV radiance differences at the individual TOMS wavelengths. By far, the largest impact is at the 313-nm wavelength. This affects the A-pair ozone, which is derived from the difference between the 312-nm and 331-nm wavelengths. The A-pair ozone has been used as the absolute standard for TOMS, so, in earlier versions of the data set, the B'-pair and C-pair ozone values have been adjusted to agree with the A-pair. These results indicate that the wavelength calibration error in TOMS resulted in an initial A-pair ozone error of 3–4 percent. Also, comparisons of the TOMS–SSBUV solar flux measurements indicate that the wavelength adjustment reduces discrepancies of 2 percent–4 percent to the level of 1 percent. We expect differences in measured solar flux due to calibration errors, but we expect such differences to be smooth with wavelength. This is not a vigorous test, but it is clear in Figure 19 that the new values for the more sensitive wavelengths at 317 nm and 340 nm provide a smoother wavelength dependence after adjustment. The radiance and solar flux comparisons are complementary in the sense that the sensitivities to wavelength calibration errors are large at different wavelengths.

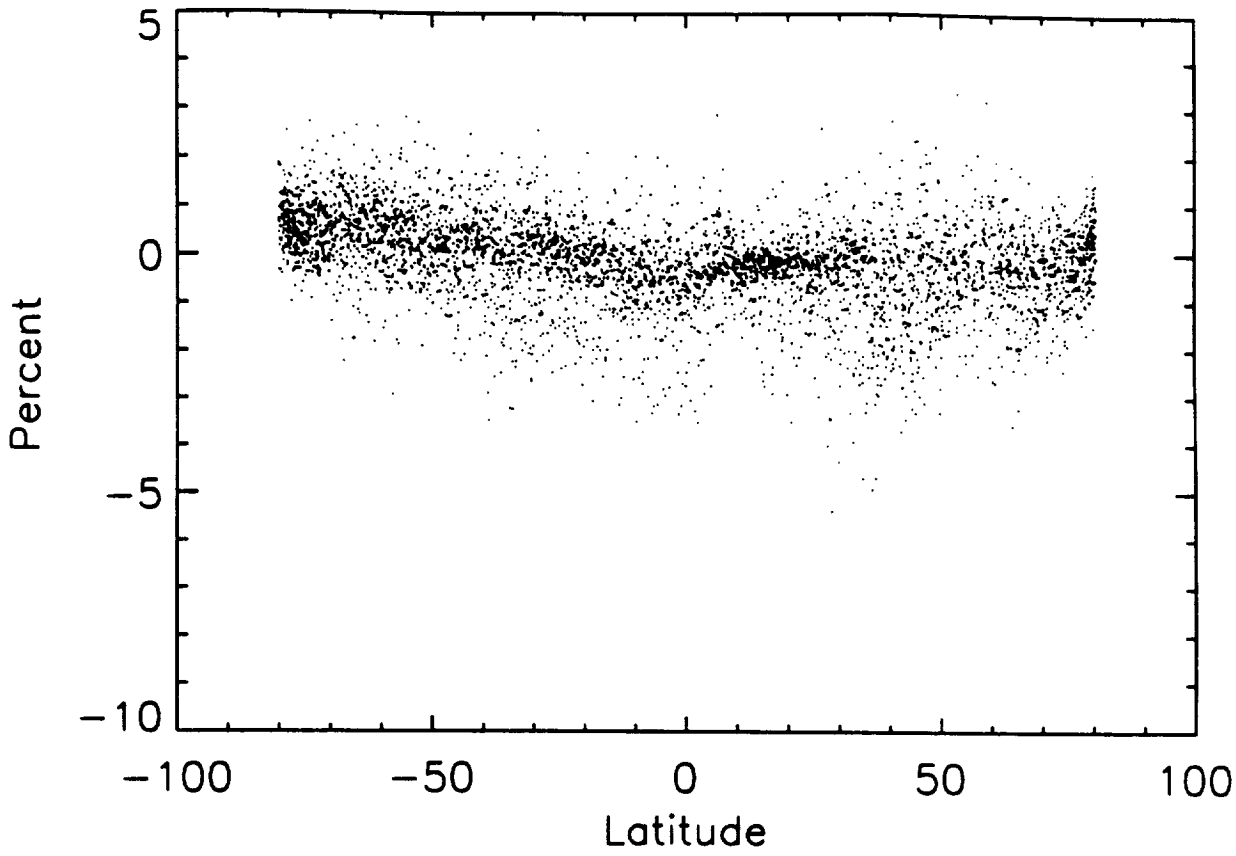

Figure 17. Corrected TOMS–SBUV percent difference in A-pair radiances for individual coincidences on March 19, 1980. The 1 percent decrease in A-pair radiance is roughly equivalent to the 1 percent increase in derived total ozone.

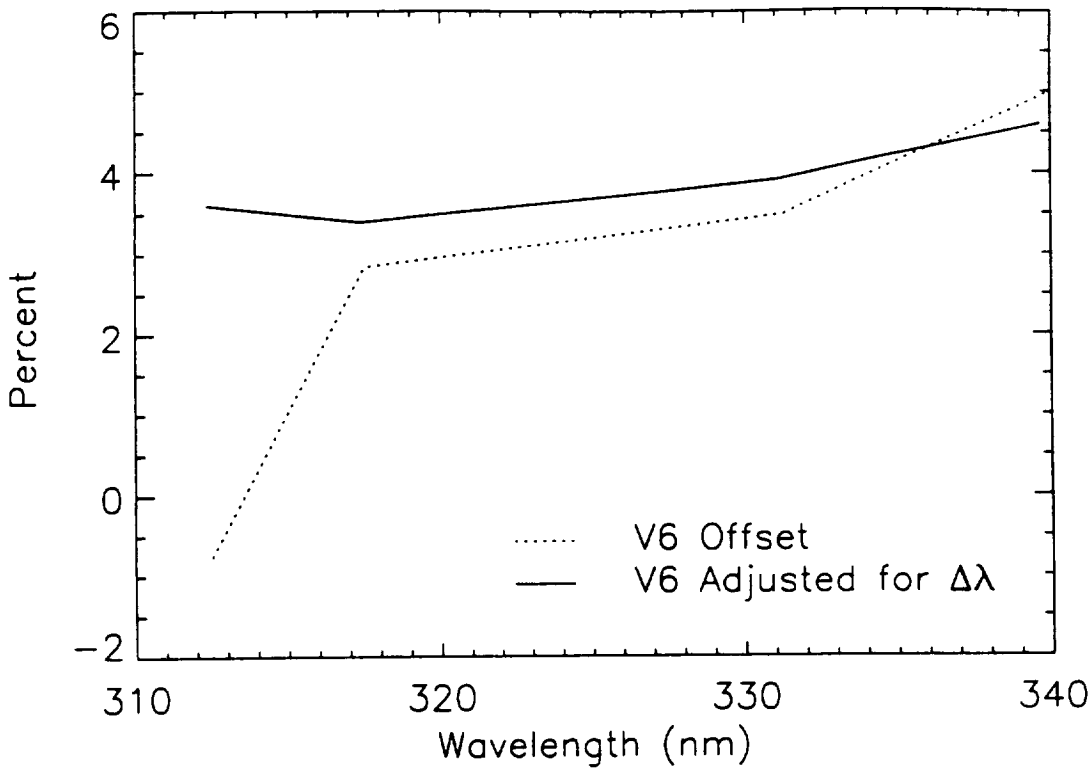

Figure 18. Initial offset in normalized radiance calibration of TOMS–SBUV shown for corrected and uncorrected TOMS wavelength calibration.

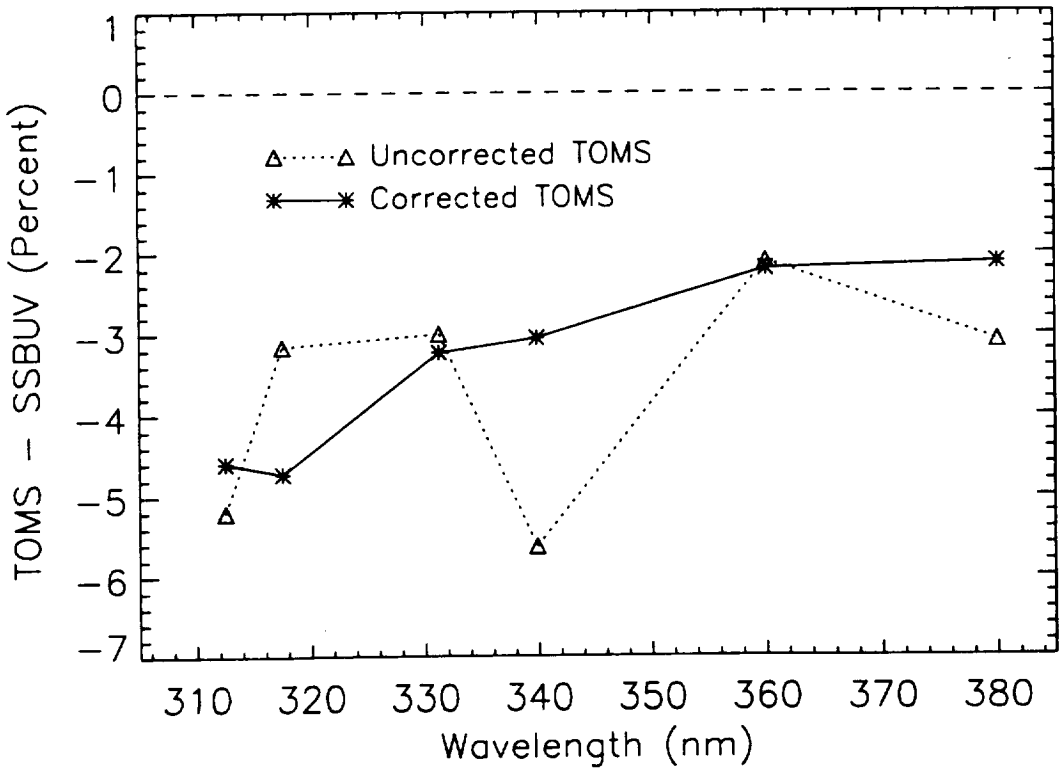

Figure 19. Impact of TOMS wavelength calibration adjustments on solar flux comparisons with SSBUV. Wavelength calibration adjustment "smooths" the calibration offset between the two instruments.

6.0 INITIAL CALIBRATION ADJUSTMENTS

Figure 18 shows the difference in TOMS and SBUV measured normalized radiances at the individual wavelength channels measured by both instruments. The difference is shown before and after adjustment for the TOMS wavelength calibration error described in Section 5. The data that have been adjusted for the wavelength calibration error show a TOMS–SBUV offset of about 4 percent at all wavelengths. The TOMS calibration at the reflectivity wavelengths is also inconsistent with the calibration of the SSBUV instrument [*Hilsenrath et al., 1995*]. This implies that it is the TOMS initial radiometric calibration that is in error. The normalized radiances that are used in the Version 7 TOMS algorithm have been adjusted, based on the TOMS–SBUV differences shown in Figure 18. An estimated adjustment of –4.2 percent is made to all wavelengths so that the wavelength dependence of the calibration is unchanged. This adjustment lowers the absolute value of the reflectivity derived using the 380-nm wavelength of TOMS by roughly 0.03 at high reflectivities and by about 0.01 at low reflectivities. As illustrated above in Figure 5, TOMS minimum ocean reflectivity provides a stable monitor of instrument calibration at the reflectivity wavelengths in absence of volcanic aerosol [*Herman et al., 1991*]. Figure 20 shows scatter plots of TOMS and SSBUV reflectivities measured over the Pacific Ocean in the range of solar zenith angles from 20 to 50 degrees. The envelope of minimum reflectivity values indicates that the reflectivity of the cloud-free ocean surface is approximately the same as measured by SSBUV and by the corrected Version 7 TOMS. This absolute adjustment to the TOMS calibration has very little effect on TOMS derived ozone, however, and because it is time independent, it has no effect on TOMS trends.

The wavelength dependence of the initial TOMS calibration has also been adjusted in Version 7. The main motivation for this adjustment is algorithmic. Since different wavelengths are used to determine total ozone in different solar zenith angle regimes, it is imperative that the wavelength dependence of the initial calibration be consistent with the forward model used to calculate theoretical radiances. Inconsistencies between the two can come about as a result of a number of wavelength dependent errors: prelaunch radiometric or wavelength calibration errors, error in laboratory measurements of the ozone absorption or Rayleigh scattering coefficients, or errors in the radiative transfer solution. The residues of the TOMS algorithm are used to determine wavelength dependent adjustments that will eliminate these inconsistencies. The residue is the difference between the measured radiance at a given wavelength and the theoretical radiance calculated using the observation geometry and the derived ozone and reflectivity. This quantity is important in the analysis of measured Earth radiances, because variability due to changes in surface reflectivity, ozone, and solar zenith angle have been removed. Modal residues from a global population sampled over all seasons are used to estimate these wavelength dependent adjustments. They are smaller than the uncertainties in the potential error sources enumerated above. The initial calibration adjustments applied in the Version 7 TOMS data are summarized in Table 4.

Table 4. Summary of TOMS Initial Radiometric Calibration Adjustments

	Adjustments to Nimbus–7 TOMS Initial Calibration (Percent)		
Wavelength	Reflectivity Adjustment	Residual Adjustment	Total Adjustment
312	–4.2	–0.2	–4.4
317	–4.2	–0.3	–4.5
331	–4.2	–0.4	–4.6
340	–4.2	–0.6	–4.8
360	–4.2	–0.2	–4.0
380	–4.2	0.0	–4.2

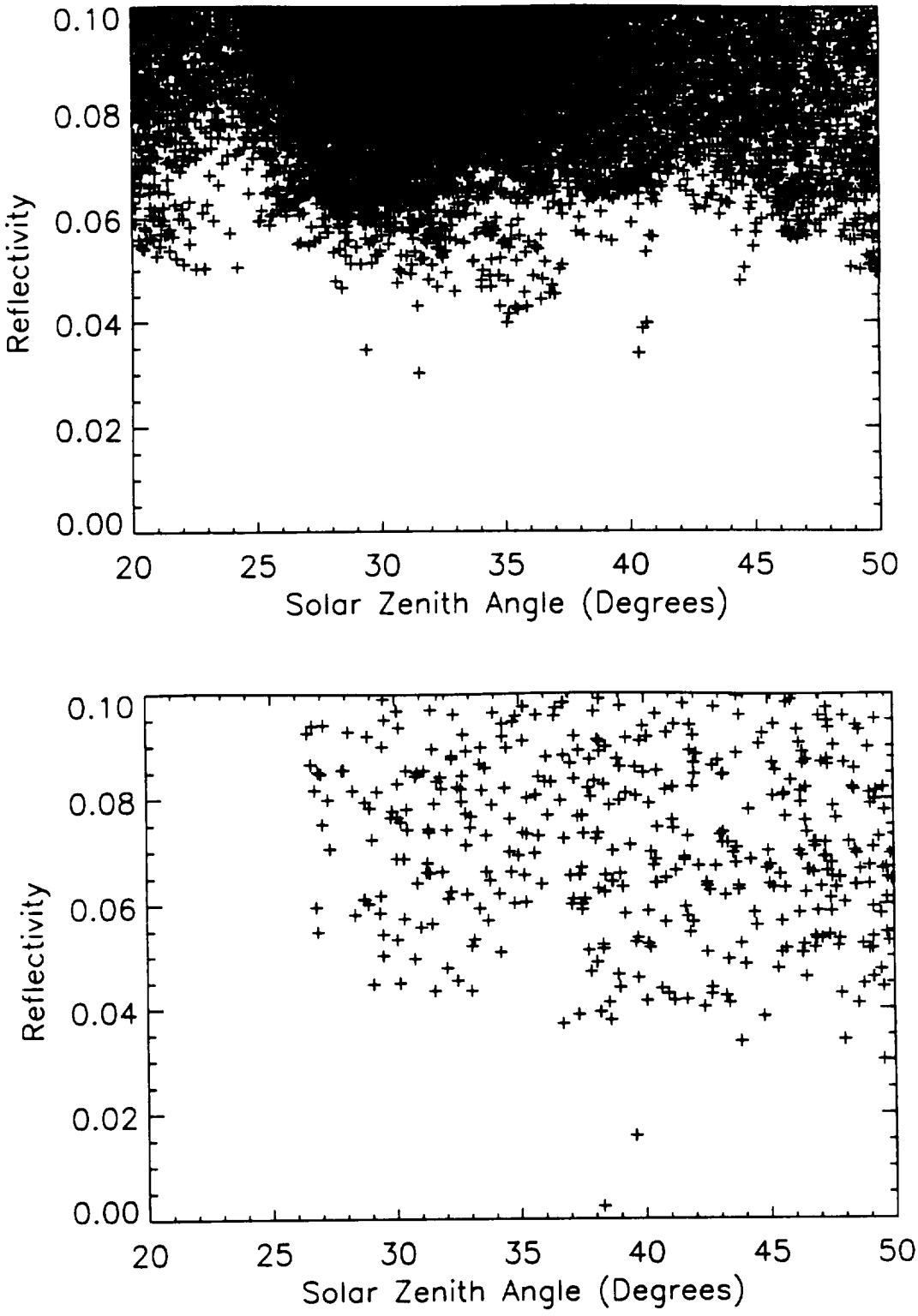

Figure 20. Scatter plots of surface reflectivity over the Pacific Ocean for a) (top) Version 7 TOMS and b) (bottom) SSBUV. The SSBUV are from Flight 5 (4/9/93–4/16/93) near the end of the TOMS data record. The TOMS data are for April 12, 1993.

7.0 IMPACT OF COPPER NON-SYNCHRONIZATION

7.1 Background

Chopper wheel synchronization errors arise from an intermittent lack of synchronization between the wavelength selection chopper wheel and the photon-counting electronics of TOMS. The chopper system is designed to remove the unwanted signal due to background radiation by counting up when the radiance signal comes through the chopper slit and counting down when the signal is cut off [*Heath et al., 1975*]. The chopper also selects wavelength. The incoming light is dispersed across the wheel so that slits milled in the wheel permit light from the selected wavelength region to pass through the exit slit to the detector. The multiple slits for each of the wavelengths of interest are interleaved to provide the sampling sequence illustrated in Figure 21. This sequence is selected to minimize the differential impact of changes in scene reflectivity on the set of measured wavelengths. The "non-sync" condition is identified by on-board electronics when it exceeds a preset threshold [*Herman et al., 1991*]. The signal is reduced by the lack of synchronization since part of the integration period (counting up) occurs when the radiance signal is cut off by the chopper wheel. Scans that are identified as non-synchronized are flagged in the TOMS orbital data set (Level-2). They are omitted from the daily averages of solar flux presented in Figure 3 and elsewhere in this report, but they are not explicitly excluded from the gridded map products (Level-3). The impact of the non-synchronized condition on the TOMS radiances and ozone is discussed further below in Section 7.3.

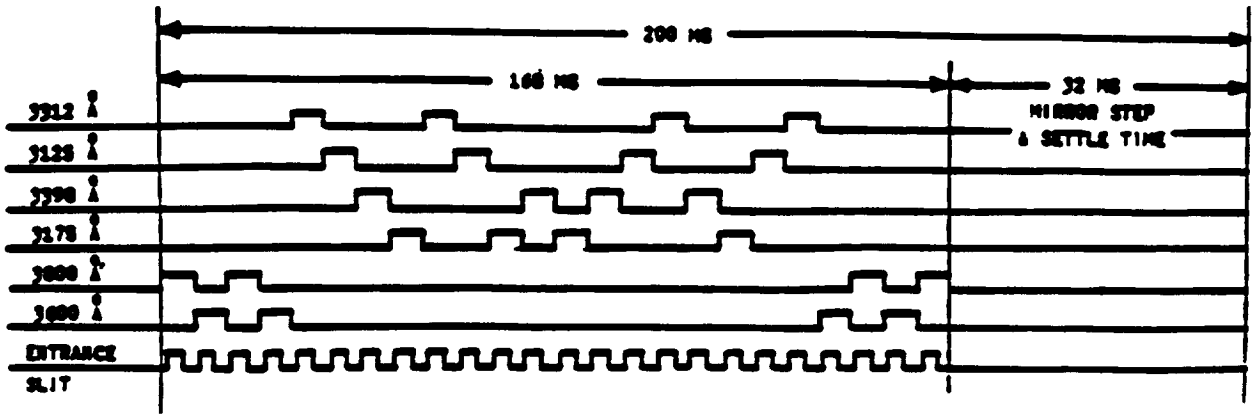

Figure 21. Wavelength measurement timing sequence for TOMS. The symmetric sampling of A-pair wavelengths (312 and 331 nm) is robust against the effects of "non-sync". (Reproduced from *Heath et al., 1975*)

7.2 "Toggling" Corrections for TOMS Radiances

Of particular interest in the correction of TOMS measurements for subsequent calibration analysis is a subthreshold synchronization error referred to as "toggling" since the instrument seems to alternate between distinct states of synchronization. These data are distinguished from non-sync data because they are subthreshold and not actually identified by the instrument as being out of synchronization. The most direct observation of the impact of toggling on the TOMS measurement can be obtained using ratios of solar flux measured at a pair of wavelengths. The A-pair wavelengths (312 nm–331 nm) are the primary TOMS wavelengths for total ozone determination. Because of this, the sampling pattern of the A-pair wavelengths is arranged to optimize robustness against changes in scene reflectivity. This design also seems to be robust against the toggling and non-synchronized conditions, and probably explains the very small impact on the A-pair wavelengths (Figure 22). The 340-nm and 317-nm channels do not exhibit the same degree of symmetry as the A-pair wavelengths, so we might expect the somewhat larger impact due to non-sync at the B-pair and C-pair wavelengths (Figure 22).

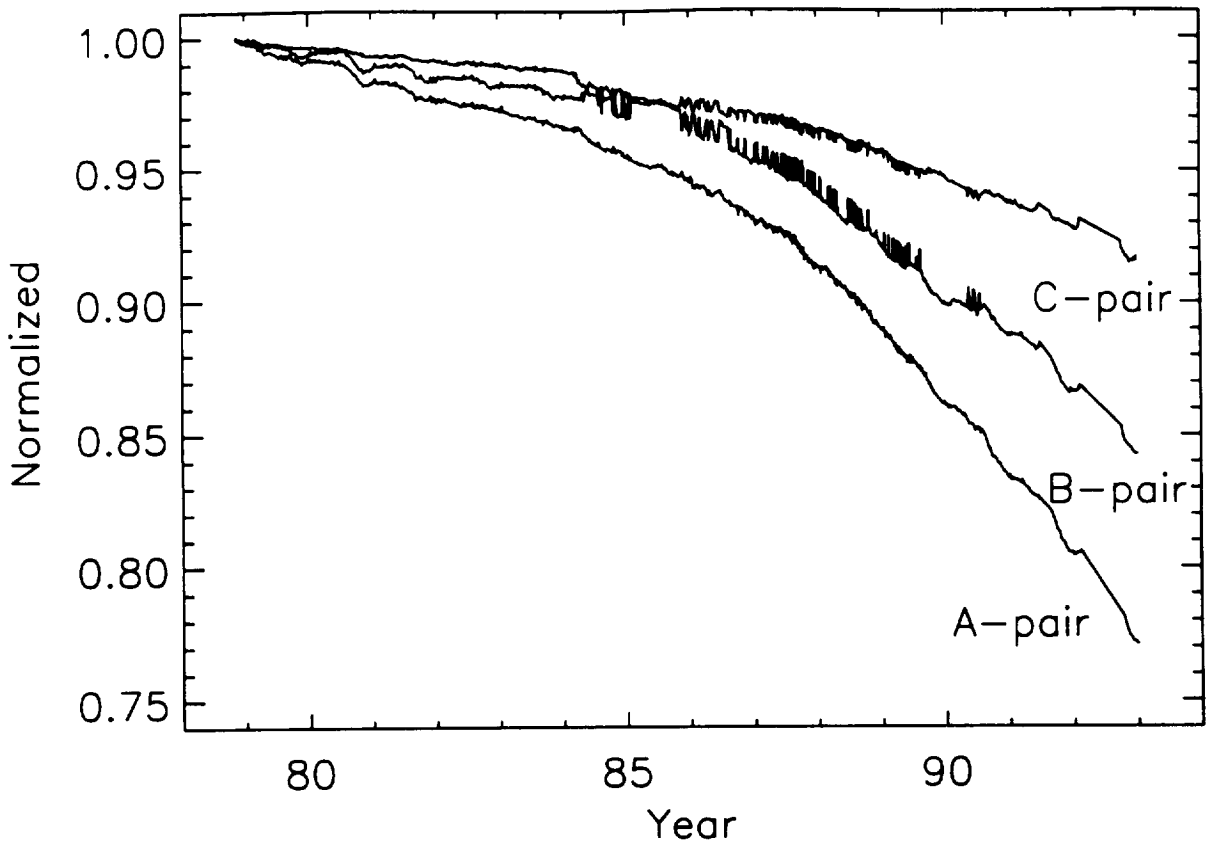

Figure 22. Ratios of TOMS solar flux measured at different pairs of wavelengths: A-pair (331 nm–312 nm), B-pair (331 nm–317 nm), C-pair (340 nm–331 nm). "Toggling" impact is not significant at the A-pair wavelengths, but is implied at 317 nm and 340 nm. See Figure 3 for individual wavelengths.

The development of a mean state correction for the toggling effect is summarized in Figure 23. Figure 23a shows the ratio of solar flux measurements at the 317-nm and 312-nm channels over the time period of 1983 through 1991. All of the non-synchronized data have been excluded from these data, which are averages of 5-minute sequences of solar measurements made periodically. The subthreshold toggling occurs sporadically over short time scales. Most of the solar averages appear to be in one state of synchronization or the other, but some intermediate average values occur indicating a change during the 5-minute measurement sequence. During fall 1990, however, the toggling ends and the instrument arrives at a final state that is different from the previous two. Instrument changes that can occur over such short time scales are inconsistent with radiance calibration techniques described in Section 2. To resolve this problem, an estimate of the toggling impact on TOMS measured radiances must be derived. It is removed for the spectral discrimination analysis and then replaced in the final estimate of instrument change. To accomplish this, the toggling impact must be identified in the Earth radiance as well as in the solar measurements.

The impact of toggling on the Earth radiance measurement is more difficult to isolate, because of geophysical variability associated with changes in ozone (Ω), reflectivity (R), solar zenith angle (θ_0), satellite zenith angle (θ), solar azimuth angle (ϕ) and pressure of the reflecting surface (P_0). This variability is taken into account using the residue of the TOMS ozone retrieval:

$$r_\lambda = I_\lambda^{meas} - I_\lambda^{calc}(\Omega, R, \theta_0, \theta, \phi, P_0) \tag{16}$$

The residue is the difference between the measured radiance at a given wavelength and the theoretical radiance calculated for TOMS using the observation geometry and the derived ozone and reflectivity. This is done using a nominal instrument calibration to provide reasonably accurate values for the ozone and reflectivity. The measured radiances with the geophysical variability removed are reconstructed by taking out the nominal calibration adjustment used. Figure 23b shows the ratio of 317-nm–312-nm daily zonal mean radiances normalized in this way

for the equatorial region. Because the A-triplet wavelengths used for ozone retrieval in the tropics are not significantly affected by toggling, the 317-nm radiances in this region exhibit the toggling impact relative to the reference 312-nm channel. This also is true of the 340-nm and 360-nm channel (not shown). Because the 380-nm channel is used to derive reflectivity, a small toggling effect at 380 nm is transmitted into the residuals at the other channels. This effect is removed using a solar-flux-based estimate of the toggling effect at 380 nm and the reflectivity sensitivity of a given channel relative to 380 nm. Also, a 0.1 percent semiannual cycle has been removed in Figure 23b to help resolve the relationship between the upper "toggled" state and the lower "normal" state.

The similarity in the toggling impact on the solar flux measurement (Figure 23a), and the Earth radiance measurement (Figure 23b) indicates that the toggling effect is indeed an instrument artifact. The solar data show long-term wavelength dependent changes due to diffuser degradation in addition to the instrument changes present in both graphs. The Earth radiances show a response to volcanic aerosols from the eruption of Mount Pinatubo in June 1991. However, both data sets indicate that the instrument arrived at third "final" state when the toggling behavior ended in September 1990.

Figure 23c shows the same data as Figure 23b with an adjustment factor of 0.9917 applied to the 317-nm radiances starting at the end of September 12, 1990, to achieve a continuous "normal" state throughout the data record. The remaining toggling signature is combined with this final state change correction to give the impact estimate shown in Figure 23d. A similar approach is used to develop corrections for the other toggled wavelengths, 340 and 360 nm. The 380-nm toggling correction is identical to the 360-nm correction except that it is scaled using a toggling impact ratio derived using the solar flux measurements at 360 and 380 nm. In the analysis procedure described in the Section 2, the toggling error signature is removed from the TOMS radiances used in the analysis and then put back into the final estimates of the instrument change.

The accuracy of this toggling correction is more than adequate for the problem of determining the long-term trend in TOMS. The critical element here is the determination of the offset in the final state from the normal initial state. This is accomplished to far greater accuracy than the 1.5 percent overall uncertainty in the quadratic determination of the instrument change at the ozone channels.

In terms of the uncertainty in TOMS derived parameters, the toggling correction is good in a mean sense, but when toggling occurs on time scales shorter than one day, the assumed state will be the weighted equatorial average of the two states rather than a single correct state. The correlation between the solar measurements and the Earth radiance measurements in Figure 23 is quite good. Areas that lack correlation indicate toggling at short time scales which is not accurately addressed by this correction. However, this technique comes very close to halving the uncertainties present in the uncorrected data even when toggling occurs on short time scales. The estimated uncertainties in individual retrievals due to toggling in the corrected data are given in Table 5. The uncertainty in individual retrievals during periods when toggling events are widely spaced in time are very small. The uncertainty in zonal means due to toggling is very small under all circumstances.

7.3 Impact of Non-Sync Condition

Figure 24 shows the daily percent frequency of TOMS non-sync measurements in the Earth radiance mode. The condition first appeared in early 1984 and became extreme in the summer of 1990. The condition abated in 1991 and then intensified again in 1993. The end of the TOMS data record occurs on May 6, 1993, when the chopper wheel actually stopped and ended the experiment. As mentioned in Section 7.1, the non-sync Earth view data are identified by flags on the TOMS Level-2 orbital product, but not explicitly excluded from the averages archived in the TOMS Level-3 gridded map product.

The best way to study the impact of non-sync on the TOMS measurement is to examine the solar measurements. In solar measurement mode, the TOMS scan mirror is stationary such that the solar diffuser is viewed, and each of the 35 samples of a scan represent a set of solar measurements for each wavelength. The solar measurement takes about 5 minutes during which approximately 1,300 samples are taken at each wavelength. The dependence of the solar signal on the incidence angle of the Sun on the diffuser is taken into account using a goniometric correction based on preflight measurements of this angular dependence. Figure 25 shows two 70-sample sequences (16 seconds) of solar

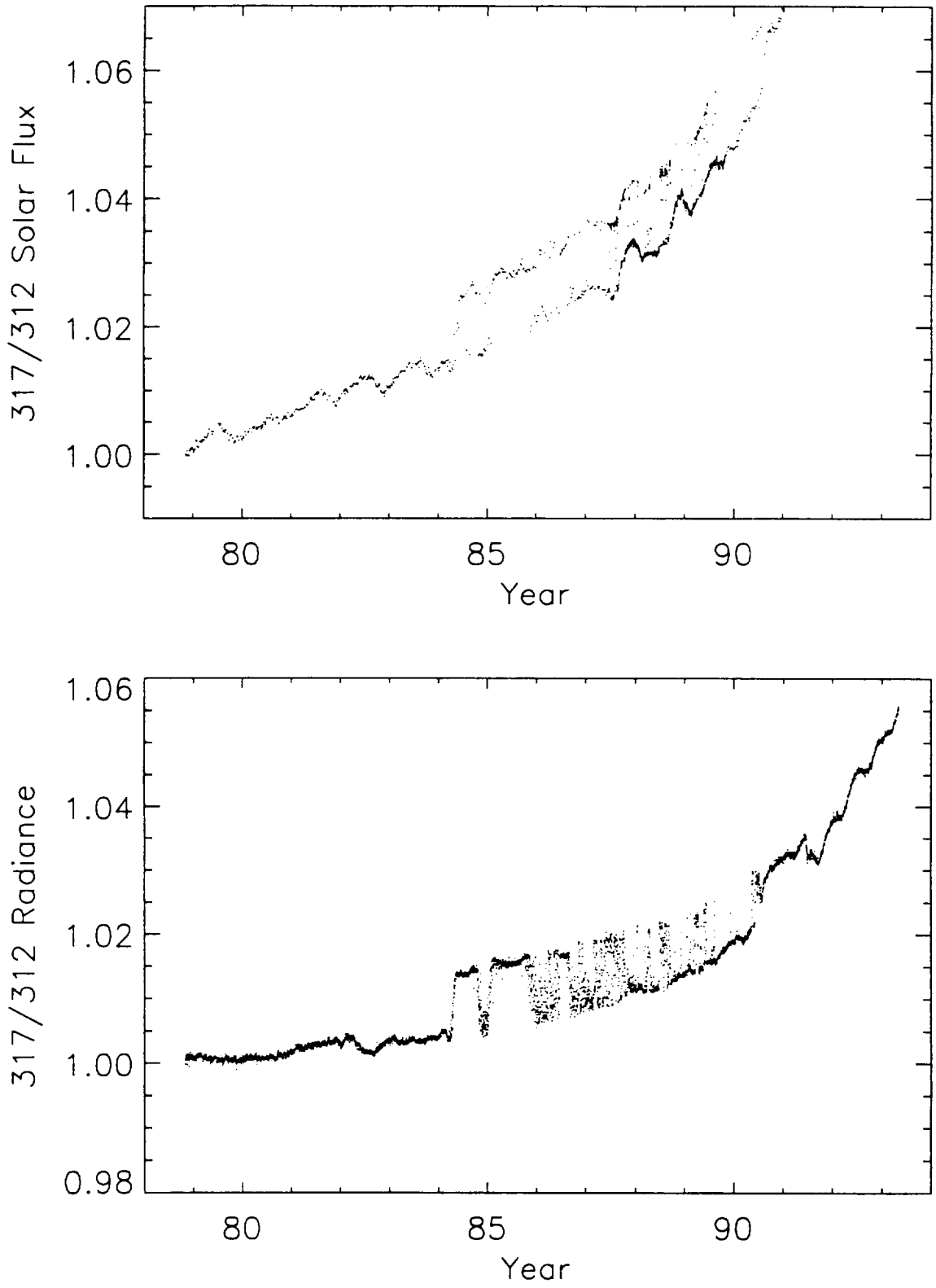

Figure 23. The development of a "toggling" correction for the TOMS 317-nm channel over the time period 1984–1990 is illustrated. a) (top) The ratio of TOMS solar flux measured at 317 nm and 312 nm show toggling impact also observed in b) (bottom) the ratio of TOMS measured radiances at 317 nm and 312 nm.

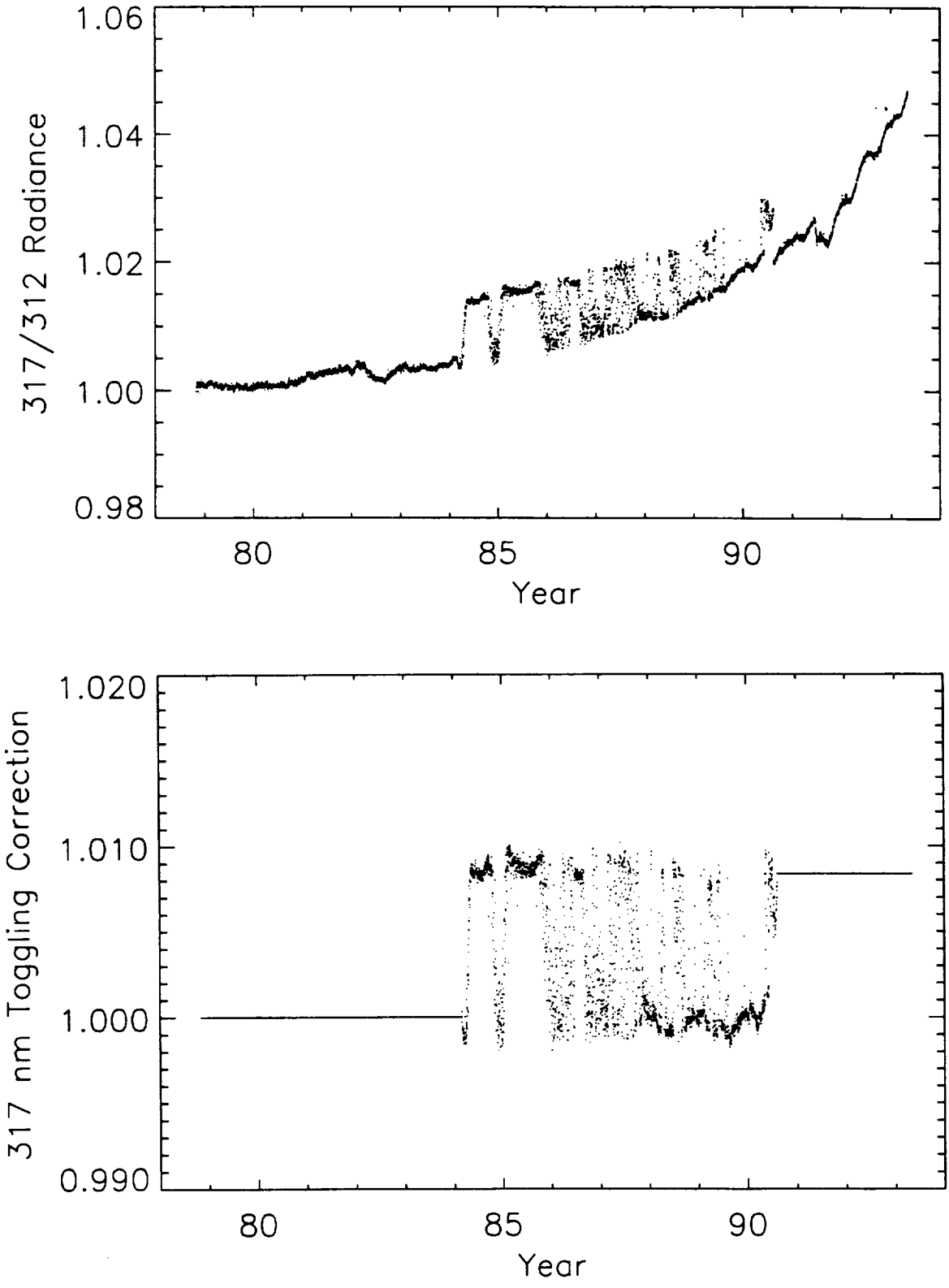

c) (top) The same TOMS radiance ratio is adjusted for the change in synchronization state on September 12, 1990, and the remaining short-term instrument changes are combined to form d) (bottom) the total estimated impact of "toggling" on the TOMS 317-nm channel.

Table 5. Impact of Short-Term "Toggling" on TOMS Derived Parameters

Impact of Short-Term "Toggling" Events on TOMS Derived Parameters			
Ozone Triplet	Wavelengths (nm)	Pathlength Region (atm-cm)	Added Uncertainty
A-triplet	312, 331, 380	0-1	0.2 D.U.
B-triplet	317, 331, 380	1-2.5	3.0 D.U.
C-triplet	331, 340, 380	2.5<	7.0 D.U.
Reflectivity	380		0.001

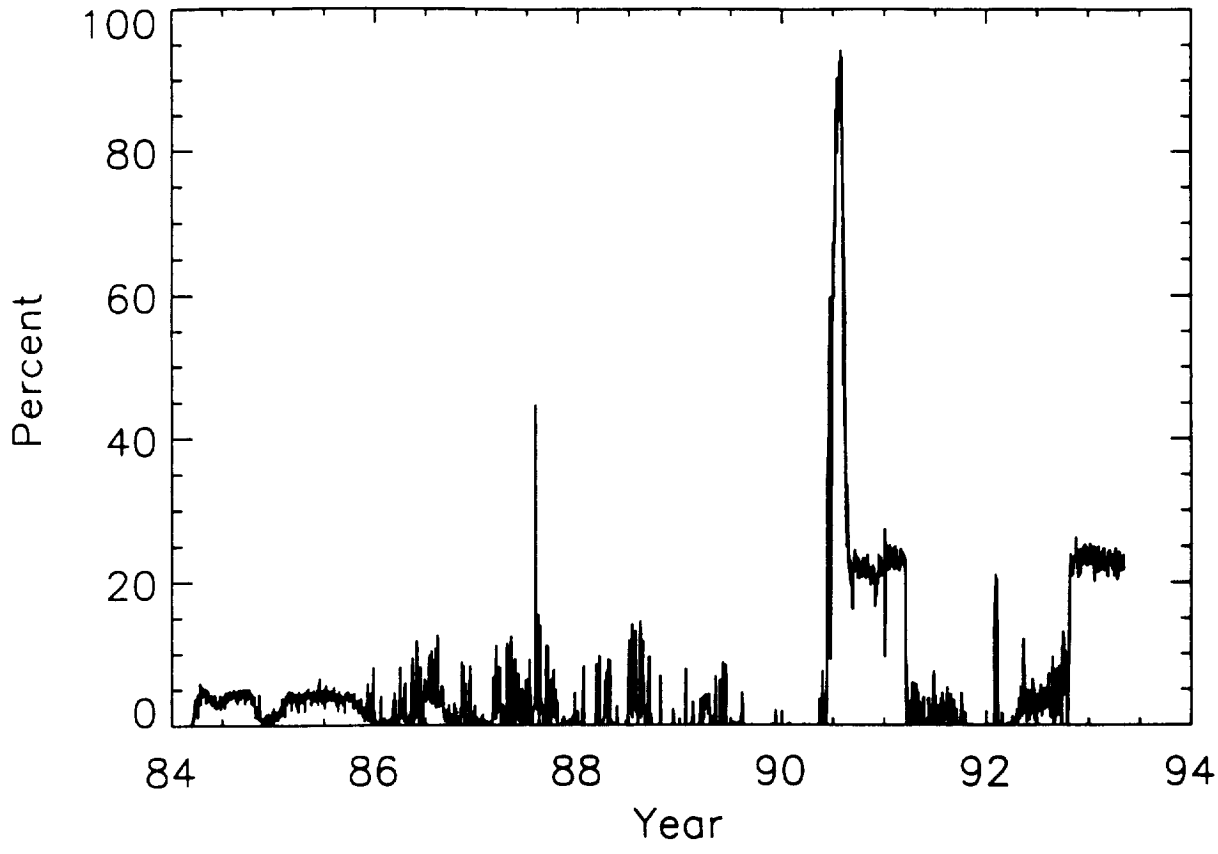

Figure 24. Daily frequency of TOMS chopper wheel "non-sync" condition.

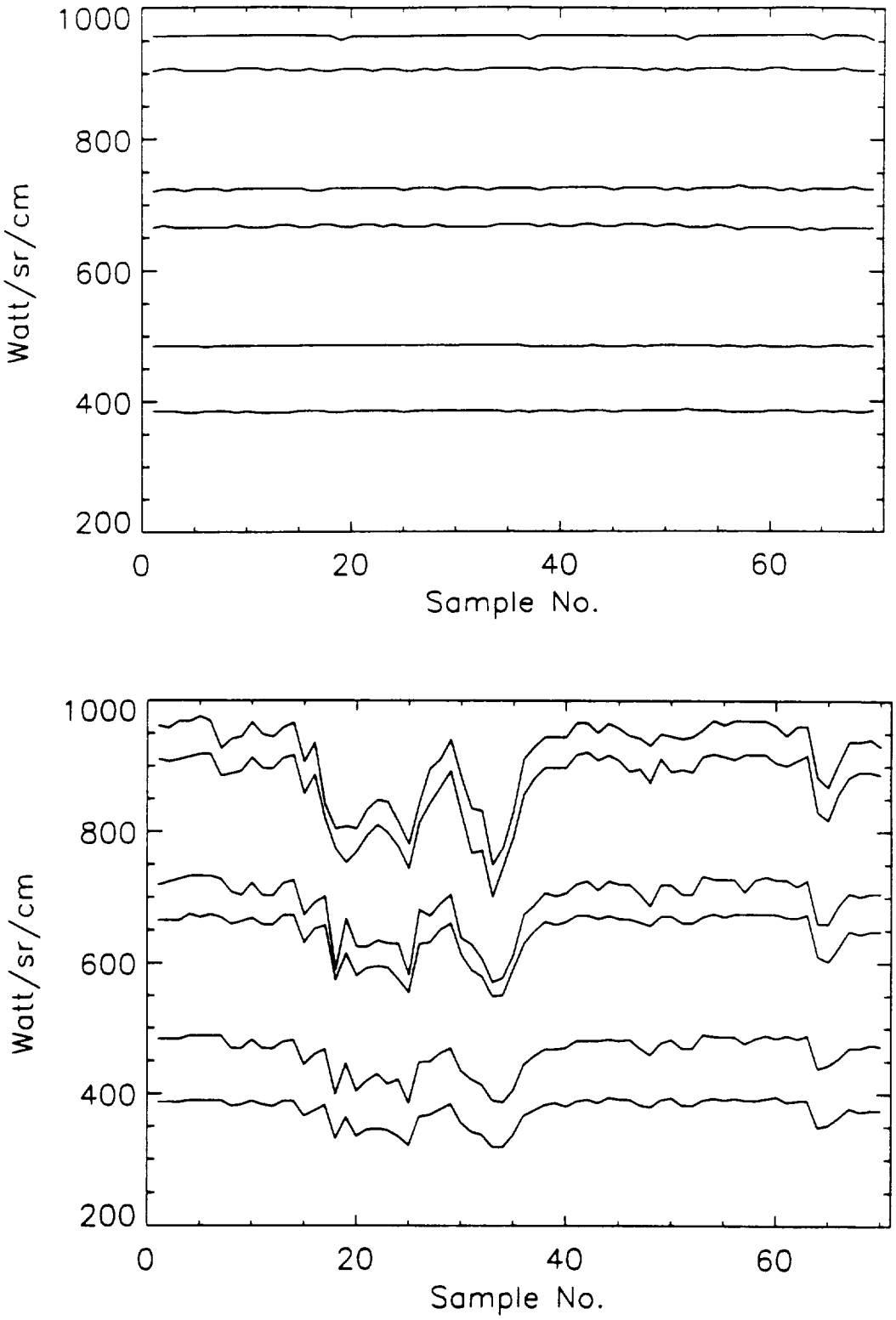

Figure 25. TOMS solar flux measurements for a single scan on a) (top) July 18, 1990, for "in-sync" condition and b) (bottom) August 8, 1990 for "non-sync" condition. The six TOMS wavelengths are ordered from long to short in the Figure from top to bottom.

measurements made during the summer of 1990 for a) "in-sync" conditions and b) non-sync conditions. Figure 25b shows strong depressions in the solar signal due to the non-sync condition, but these depressions do not show a strong wavelength dependence. This is the result of the design of the instrument in which the sampling of the wavelengths is interleaved as discussed above in Section 7.1. As also noted above, we expect smaller impact due to non-sync across the A-pair wavelengths than at the B-pair or C-pair wavelengths (Figure 21). The 380-nm reflectivity channel is used in conjunction with each of these pairs in the Version 7 retrieval, but as noted in Section 2.2, the triplet formulation is insensitive to errors at the 380-nm reflectivity channel.

The impact of non-sync errors on derived ozone is estimated by assuming that errors similar to those observed in the solar flux are present in the Earth radiance measurements. The errors taken from each of the solar samples in Figure 25b are propagated through the retrieval algorithm for a single day of data, and the resulting biases for the equatorial region are shown in Figure 26. The error is limited by internal checks on the residue of the Version 7 algorithm. In regions where the non-sync impact is large, the population of retrievals has been reduced dramatically by these checks. Population reductions of this order are not observed in the Version 7 data record. The only significant rejection rates due to non-sync occur when the non-sync frequency is larger than 25 percent during the summer of 1990. When the non-sync frequency peaks at 95 percent near the beginning of August 1990, the algorithmic rejection rate also peaks at 15 percent. So, the nominal non-sync impact must be smaller than the case depicted in Figure 25, and the occurrence of errors as large as those depicted in Figure 26 must be quite rare. These upper bounds on the uncertainty in ozone as well as the results of a similar analysis of reflectivity are given in Table 6. Although errors of this magnitude may occur in the TOMS data, very few will pass the algorithm checks and be included in the Level-3 map product.

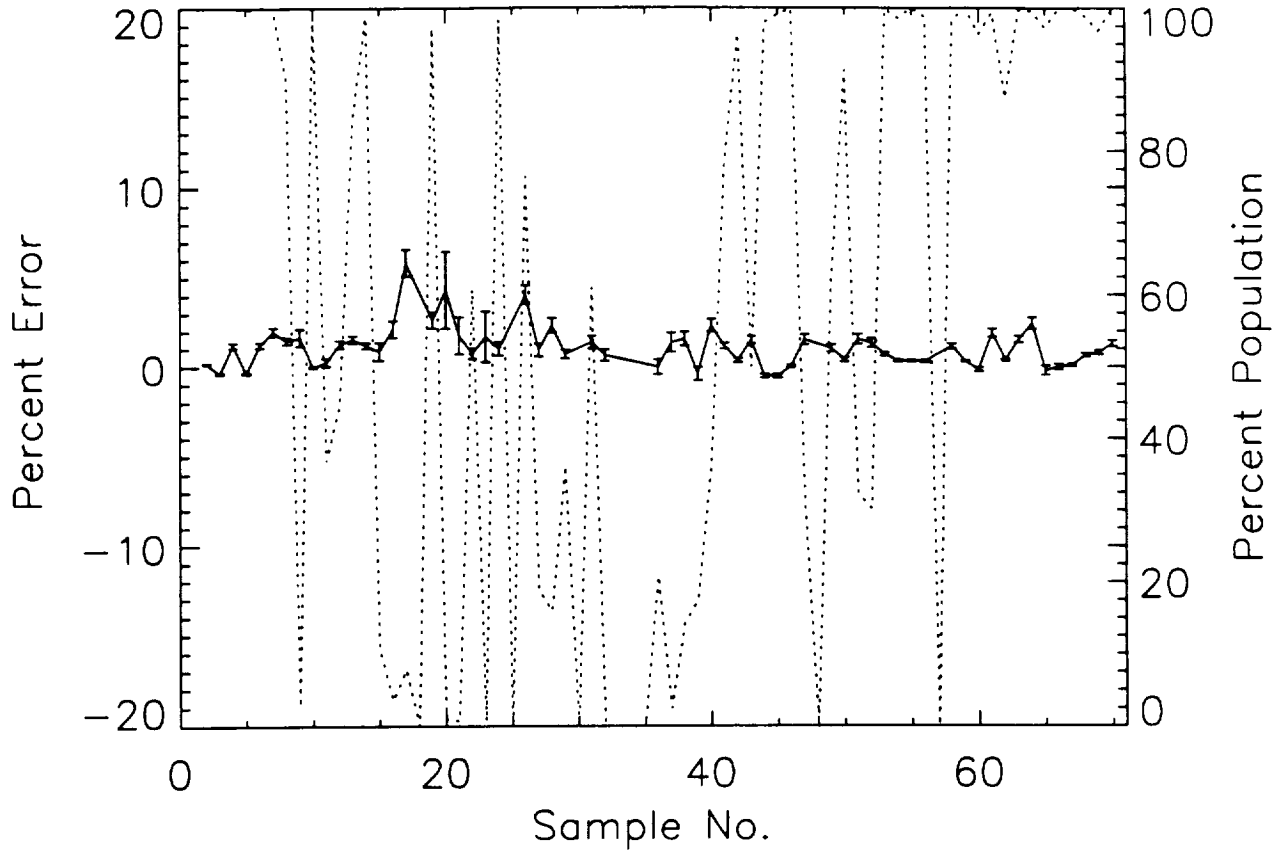

Figure 26. Estimated impact of "non-sync" errors on TOMS retrieved total ozone for the equatorial region. Percent of sample day's population not flagged for bad radiances by the TOMS algorithm is also shown (dotted line).

Table 6. Worst Case Impact of "Non-Sync" on TOMS Derived Parameters

Latitude Region (Degrees)	Uncertainty in Ozone (Percent)	Uncertainty in Reflectivity
<30	6	0.15
30–60	9	0.10
60–90	11	0.40

8.0 OTHER INSTRUMENT PERFORMANCE ISSUES

8.1 Evidence of Hysteresis in TOMS

The SBUV monochromator has a reference detector called the reference photodiode channel. The data from the reference channel can be used to compensate the data from the monochromator for changes in PMT gain. This reference detector uses a beam divider mirror to divert a small fraction of the PMT input to the reference photodiode. The reference photodiode consists of a bare photocathode that is identical to the photomultiplier tube's photocathode. Hence, the spectral response of this device is matched to that of the PMT. The field of view is also the same, but the mirror changes the energy distribution across the field of view so, the bandpass may be somewhat different. The reference photodiode channel is only usable at high light intensities, since it only deals with one tenth of the monochromator output signal and the detector has an electronic gain of only one [*Beckman, 1980*].

The SBUV is known to have a problem with hysteresis associated with a "warm-up" period after it comes past the southern terminator into the sunlight each orbit [*Bhartia, et al., 1995*]. The SBUV measured radiances can be corrected using the reference photodiode, however, and can be compared with the TOMS. The results of such a comparison are shown in Figure 27. Here, a similar hysteresis is indicated in TOMS. Similar comparisons done at different times however, do not indicate any significant time dependence of the hysteresis in TOMS. The hysteresis is not wavelength dependent, so it has no significant effect on TOMS total ozone. A difference of about 0.05 in reflectivity is observed, however, between observations of highly reflective scenes in the Northern Hemisphere and those near the terminator in the south.

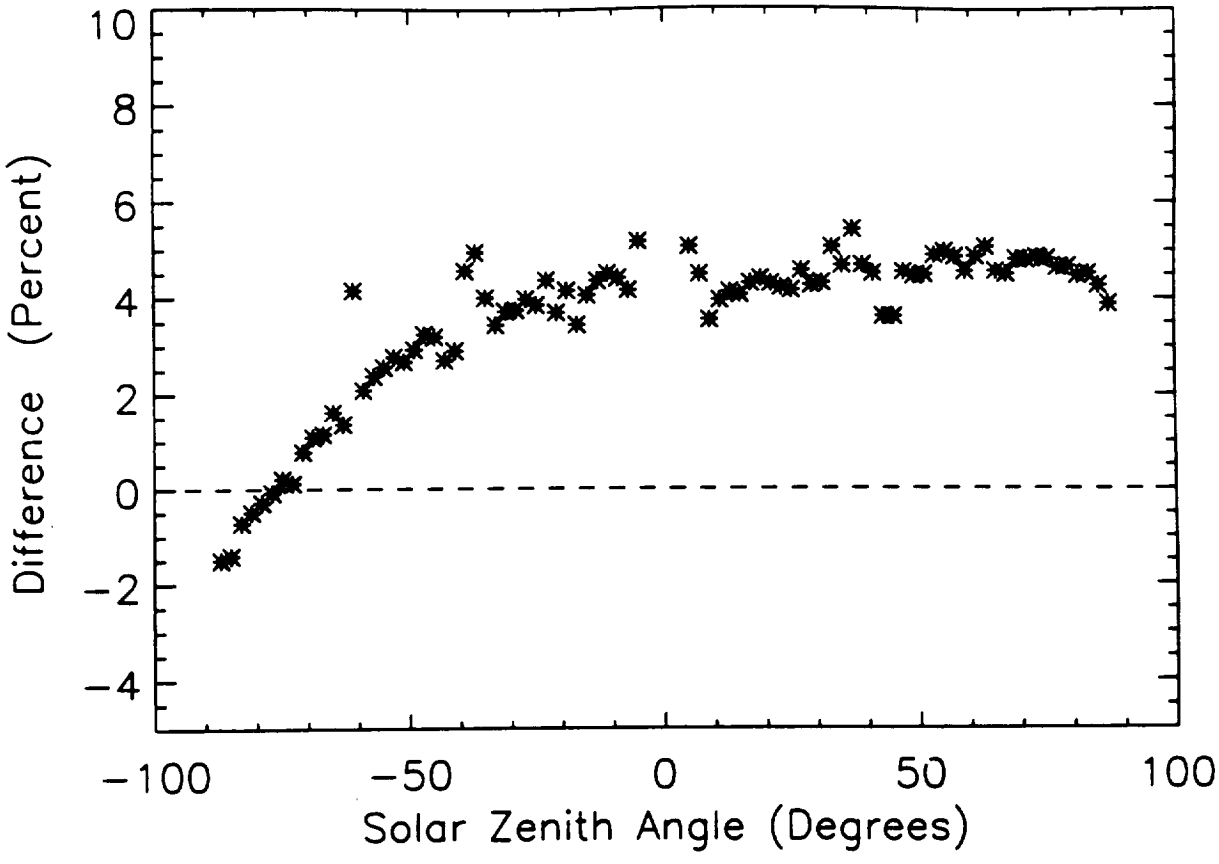

Figure 27. TOMS–SBUV radiance difference at 340-nm channel using corrected SBUV data for March 20, 1979. Evidence of hysteresis in TOMS associated with emergence into light at the southern terminator. This effect is neither wavelength nor time dependent. (In Figures 27 and 28, negative values of solar zenith angle indicate measurements from the Southern Hemisphere with positive solar zenith angles.)

Figure 28 is similar to Figure 27 except that it is for March 20, 1990, near the end of the data record. This later comparison shows an added effect in both hemispheres. This appears to be a signal level dependence in TOMS relative to SBUV that has developed over the course of the experiment. Our analysis of this effect is presented in the next section.

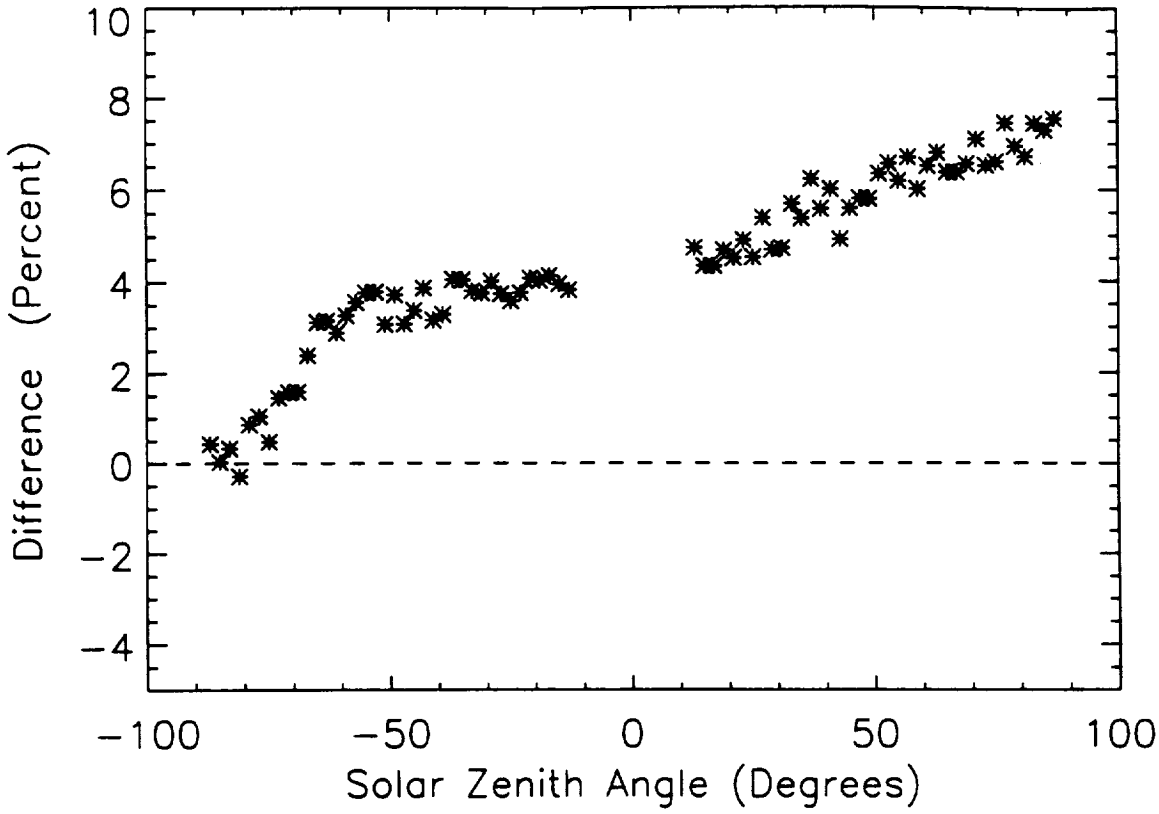

Figure 28. TOMS–SBUV radiance difference at the 340-nm channel using corrected SBUV data for March 20,1990. Possible signal level dependence indicated in Northern Hemisphere. Southern Hemisphere exhibits the combined effects of hysteresis and signal level dependence.

8.2 Signal Level Dependence Relative to SBUV

Additional evidence of a small signal level dependence in the TOMS photomultiplier comes from radiance comparisons with the SBUV instrument as described in Section 4, incorporating the wavelength calibration corrections discussed in Section 5. The results of this comparison are shown in Figure 29 as scatter plots of individual TOMS–SBUV coincidences over a 5-day period in March 1985. These results indicate a signal level dependence in the TOMS instrument of 3–4 percent. The dependence looks linear as a function of the logarithm of signal level (Figure 29b). In Figure 29c, however, the unusual nature of this dependence is revealed as the error grows faster at lower signal levels.

Figure 30 illustrates further insight of this phenomenon gained by binning the radiance comparison data by signal level. Figure 30a showing data from 1980 shows no signal level dependence at low signals (high N-value), but does show a saturation type effect at high signal level (low N-value). If this initial signature is subtracted from the results of subsequent years (Figure 30b for 1990), a "hockey stick" dependence is revealed. The "blade" of the hockey-stick is at high signal (low N-value) where no time-dependent error exists. The blade is attached to the "handle" which extends downward toward lower signal levels (high N-value). This is consistent with the results of similar analysis for intervening time periods indicating that the saturation effect is constant in time, and that the signal level dependence at low signal levels has a threshold value of approximately 125 N-value units and a linear slope that is time dependent.

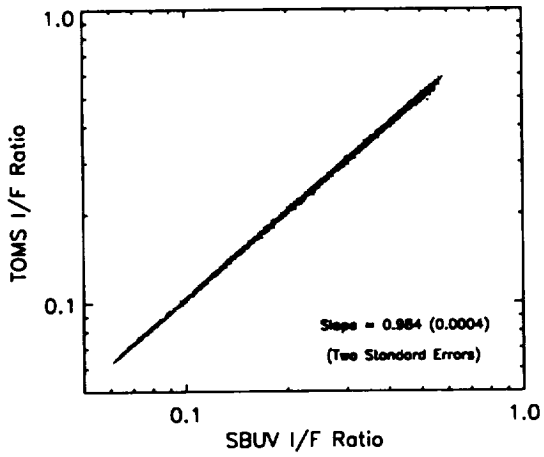

a) Correlation plot of TOMS and SBUV normalized radiances shows a small but significant slope.

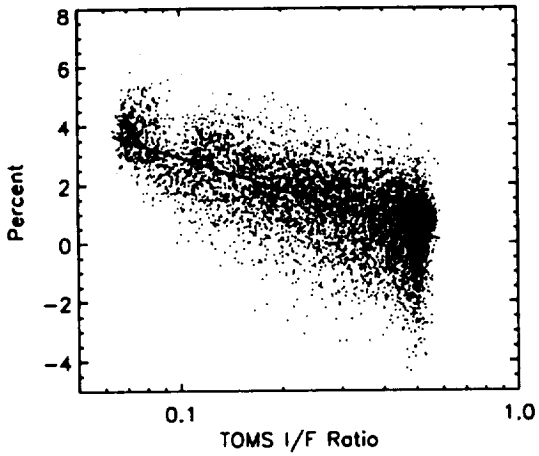

b) Percent deviation from linearity is roughly linear with the log of normalized radiance or log of count rate.

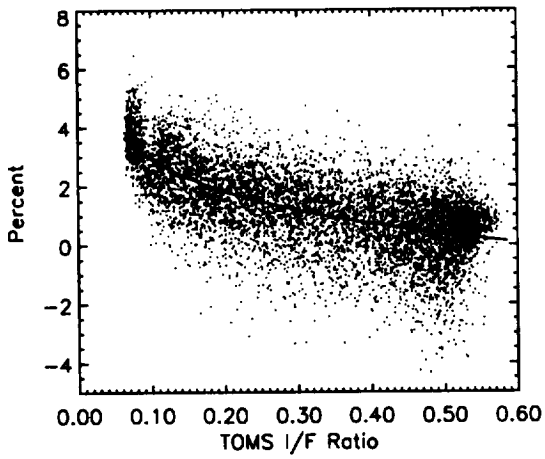

c) Signal level dependence exhibits unexplained behavior at low signal levels.

Figure 29. Evidence of signal level dependence in TOMS radiance measurement relative to SBUV. Data are from a five day period in March, 1985.

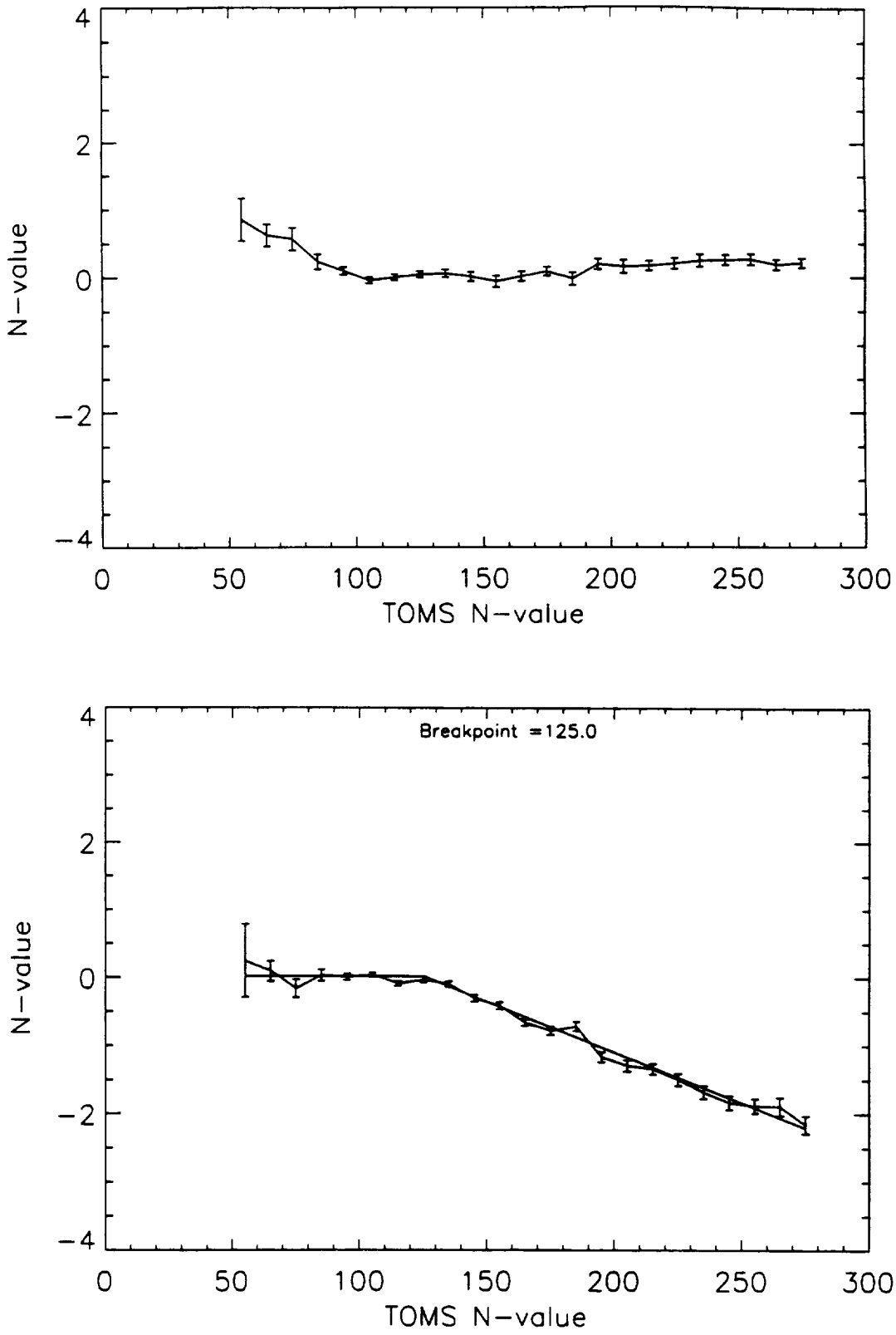

Figure 30. Binned data for a five-day period in March of a) (top) 1980 and b) (bottom) 990 showing "hockey-stick" behavior in implied signal level dependence. Data for 1990 are normalized by subtracting the 1980 behavior.

Figure 31 shows the results of linear regression based on a hockey-stick model applied to eighteen 5-day periods selected to characterize the TOMS-SBUV overlap period. The change in slope with time is shown to be approximately linear with a slope of –0.0017 and a 95 percent confidence limit of about 0.0002. The SBUV comparison data are not available after 1990. The figure also shows results of Meteor–3 TOMS comparison made in an attempt to corroborate the signal level dependence implied by SBUV.

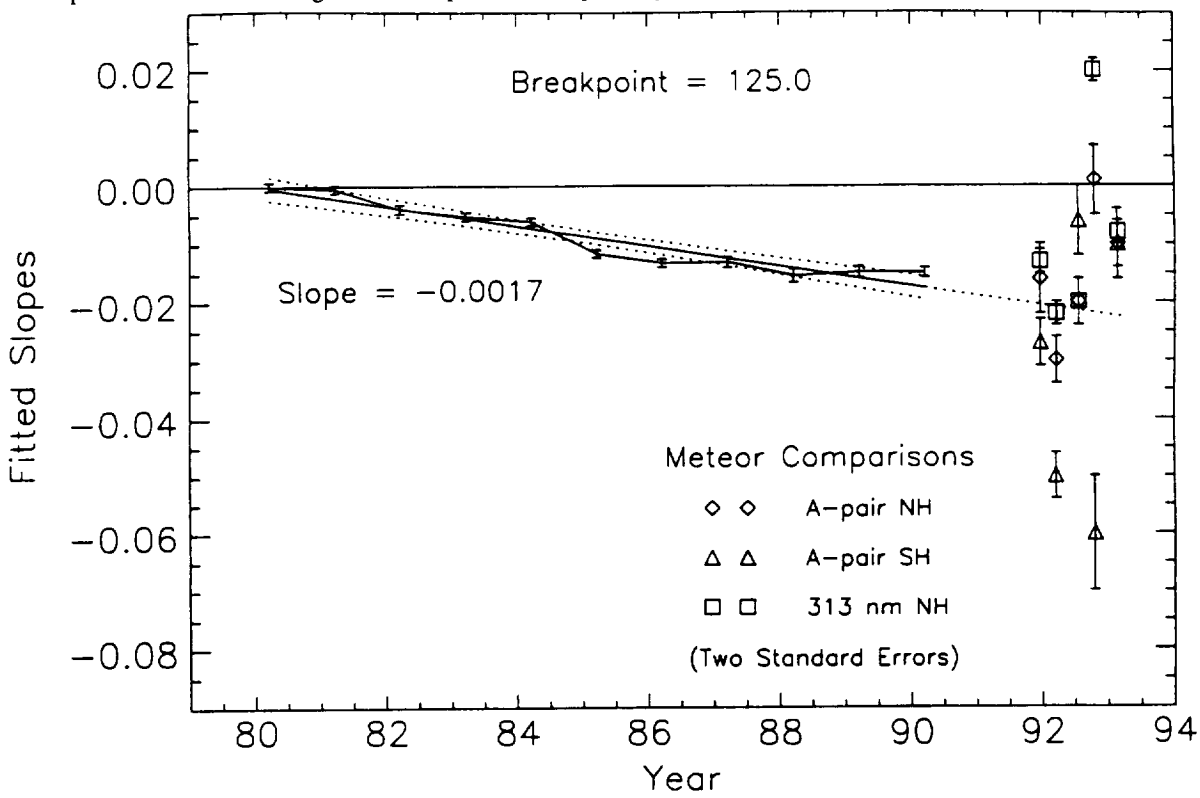

Figure 31. Slopes derived by regression of signal level dependence for each of eighteen 5-day periods over the range of TOMS–SBUV comparison. Results of the less accurate Meteor–3 TOMS comparisons are also shown.

Since the Meteor–3 and Nimbus–7 TOMS fly on separate spacecraft in different orbits, no exact coincidences like those of the Nimbus–7 TOMS and SBUV can be achieved. Because of this, a different approach is used for this comparison. Meteor–3 and Nimbus–7 TOMS N-values from the 312-nm channel are fit as a function of solar zenith angle for five 10-day periods during which both satellites were in similar orbits. Then, the slope of the difference of the fits is determined for N-values greater than 125. These results seem to support the possibility that a signal level dependence exists, but no real quantitative information can be gleaned from the Meteor–3 results shown in Figure 31.

To summarize, there is some evidence that a signal level dependence developed in the TOMS. This possibility is important because it may affect the long-term ozone trend derived from TOMS, as well as the solar zenith angle dependence. The effect is small however, and it is difficult to characterize accurately. What physical mechanism might cause such a dependence is not clear, and the Meteor comparison results are not quantitative in the period after the SBUV data are no longer available. For these reasons, no correction has been made for the apparent signal level dependence in the Version 7 reprocessing of the Nimbus–7 TOMS data.

To estimate the possible impact of this error on the derived ozone, we assume that the apparent signal level dependence exists in Nimbus–7 TOMS and continues to grow at the rate indicated by the SBUV comparisons until the end of the TOMS data record in May 1993. A correction has been developed based on the hockey-stick model, and used in sample data processings to generate an impact estimate. The resulting estimate of the impact of this error on derived ozone at mid-northern latitudes and in the equatorial region is shown in Figure 32. The 2 percent impact in trend at mid-northern latitude results from the linear increase in the slope of the signal level dependence, and the growing seasonal variation results from the larger errors occurring at high solar zenith angles when signal level is low.

In the equatorial region, there is minimal effect because the signal levels remain relatively high. Since no correction is made in the Version 7 TOMS reprocessing, the impact of this error on the TOMS derived ozone trend must be considered as a possible systematic component in the error budget.

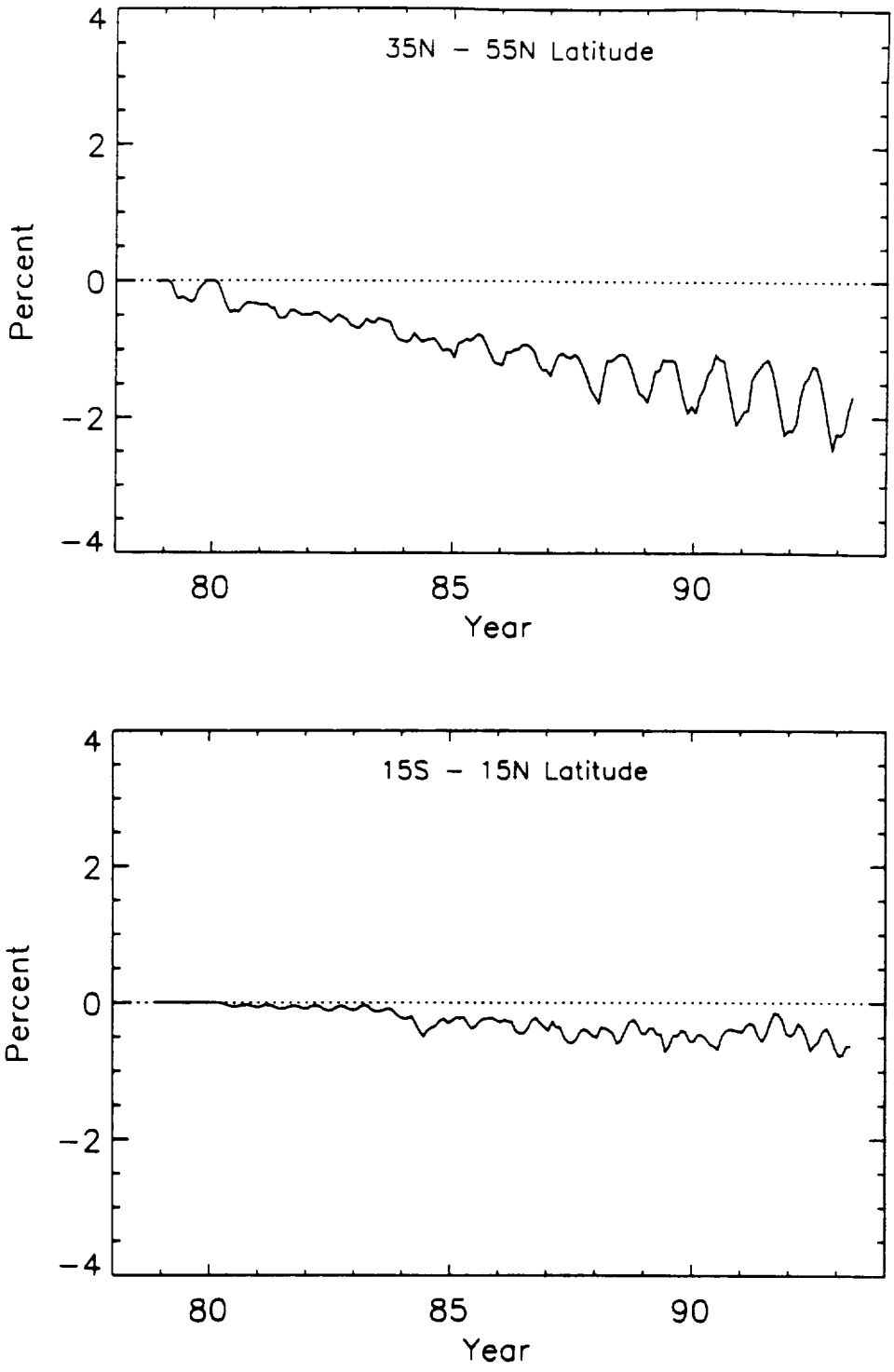

Figure 32. Error estimate for TOMS signal level dependence on total column ozone in a) (top) mid-northern latitudes (35° N–55° N) and b) (bottom) the equatorial region (15° S–15° N). The impact is larger at low signal levels during winter.

9.0 COMBINED UNCERTAINTIES

9.1 Error Analysis

A statistical uncertainty in the Version 7 Nimbus–7 TOMS derived ozone trend has been developed in Section 3, using the distribution of calibration results derived from different subsets of the TOMS radiance measurements using the spectral discrimination method. This approach yields an uncertainty of 1.5 percent over the entire data record or about 1 percent/decade. The error budget is also affected by two systematic errors. One is the possible error associated with the choice of the quadratic form to characterize the wavelength dependence in the calibration drift, which is also discussed in Section 3.4. This error is about +1 percent in ozone over the TOMS lifetime (14.5 yrs). The second error source is a possible signal level dependent error in the TOMS measured radiance that may increase with time. This error is insignificant at the equator, but may be as much as –2.0 percent at mid-latitudes and high latitudes (Section 8.2). Neither of these errors is characterized well enough to remove from the data set. They are opposite in sign and combined, remain within the limits of the statistical uncertainty, so the statistical estimate is considered to be appropriate. The uncertainty of the long-term data set as a whole then, is 1 percent/decade in derived ozone. Note that the larger systematic error source has a strong latitude dependence so that the quoted uncertainty pertains to the relationship of mid-latitude and equatorial trends, as well as the trend itself. The data before mid-1990 are more precise than this, but the increase in the rate of instrument change and its wavelength dependence make the later part of the data record less reliable and result in the quoted uncertainty.

The absolute uncertainty of the TOMS derived ozone is unchanged in Version 7. The systematic uncertainty is 3 percent due largely to uncertainty in the ozone absorption cross-sections and wavelength calibration error, with a random component of 2 percent that results from algorithmic uncertainties associated with variability in observing conditions [*McPeters et al., 1993*].

9.2 Comparisons with Independent Measurements

The uncertainty provided for the TOMS derived ozone trend is an estimate. To validate this estimate, it is appropriate to compare TOMS with other independent measurements of total ozone. Presented below are TOMS comparisons with both SBUV and Dobson measurements.

The Version 7 Nimbus–7 TOMS data set is independent of the Version 6 Nimbus–7 SBUV data set. To develop a comparison that will provide insight into calibration differences between the two instruments, the TOMS data are restricted to near nadir retrievals to remove the impact of possible algorithmic differences associated with the TOMS scanning feature. Figure 33 shows comparison results for selected monthly zonal means for the period of TOMS–SBUV coincidence. The initial bias is within the 1 percent uncertainty in wavelength dependent calibration. Note that a wavelength independent calibration adjustment has been made to the TOMS, but no adjustment was made to the wavelength dependent calibration other than the wavelength scale adjustment which has resolved discrepancies in earlier comparisons of ozone from the two instruments. The drift in bias at the equator is not within the uncertainty of the TOMS calibration developed in this work. Similar calibration and algorithmic techniques must be applied to the SBUV data to understand this difference. The latitude dependence in the drift is consistent with the signal level dependent difference in SBUV and TOMS discussed in Section 8.2.

The TOMS Version 7 data have been compared with ground-based measurements made by a network composed of 30 mid-northern latitude stations. The stations were selected by a data coverage criterion requiring homogeneous coverage over the 14.5-year lifetime of TOMS. Differences of individual coincidences within ±1 degree for all reporting stations were averaged weekly to provide the time series shown in Figure 34. Both the TOMS and ground-based ozone retrievals are based on the same absorption cross-sections [*Paur and Bass, 1985*], so we expect the bias to be within the combined uncertainties of the comparison technique and the TOMS and ground-based measurements. This is true throughout the time series except in the winter of 1978–1979. During this initial period, there is a rapid change in the TOMS instrument sensitivity that may not be characterized properly. The standard deviation of the weekly mean biases in this period do not increase drastically. This indicates consistency within the ground based measurements, and implies that TOMS is the likely source of this difference. Apparent discontinuities near the end of 1982 and in mid-1988 do not correspond with known events in the TOMS history. The cause of these small discontinuities is unknown.

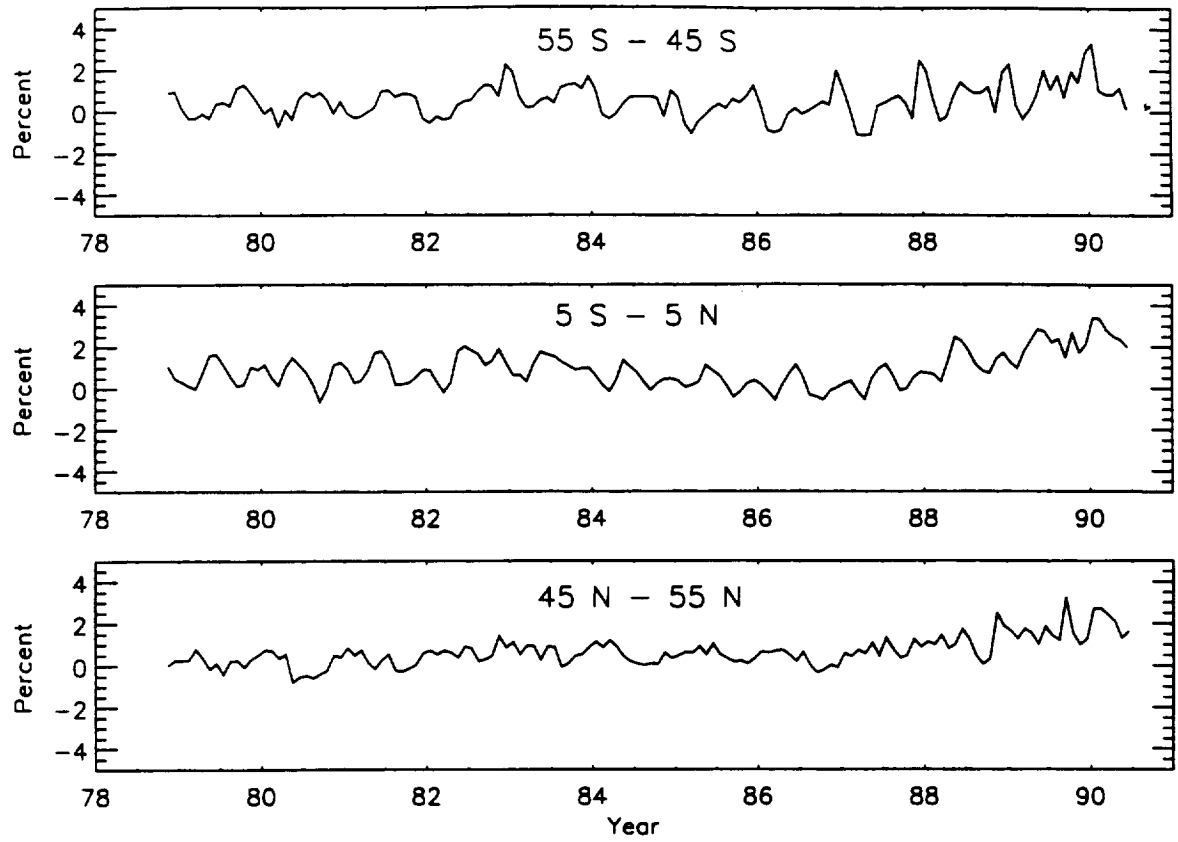

Figure 33. Version 7 TOMS, Version 6 SBUV difference in monthly zonal mean ozone for selected latitude zones.

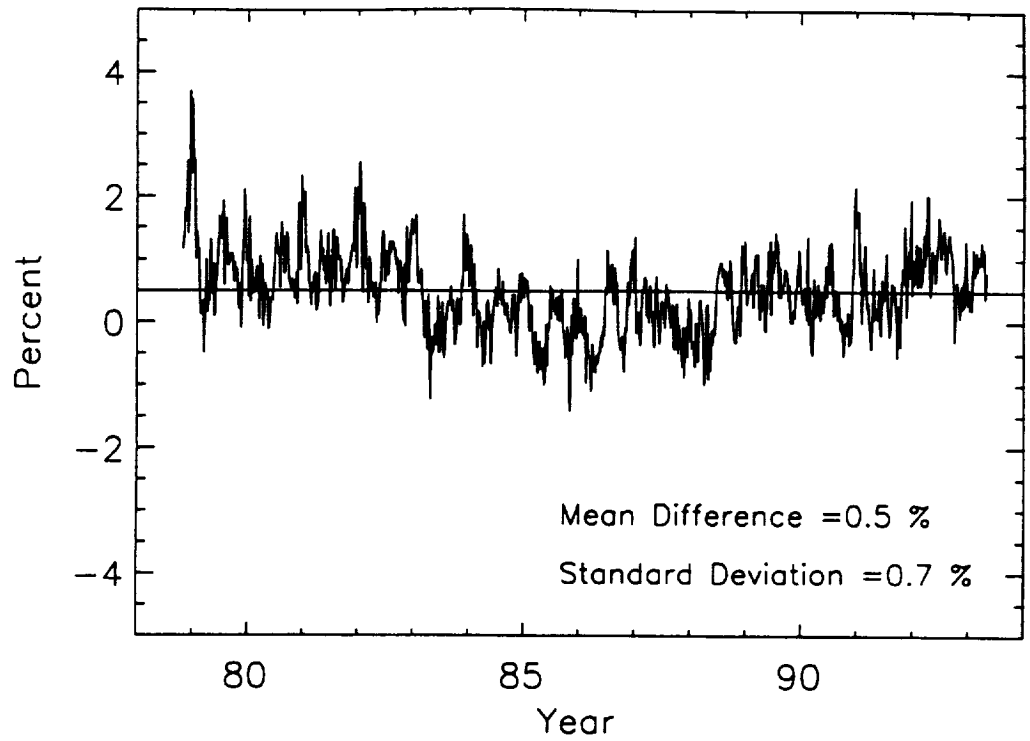

Figure 34. Version 7 TOMS, Dobson differences for 30 mid-northern latitude stations. Weekly means of differences from individual matchups at all reporting stations are plotted.

10.0 CONCLUSIONS

The long-term calibration of the Nimbus–7 TOMS has been determined over the 14.5-year lifetime of the instrument using spectral discrimination, an independent internal calibration technique. The uncertainty in this determination is 1 percent/decade in ozone. The initial ozone value is improved by corrections to the TOMS wavelength scale based on a re-analysis of prelaunch wavelength calibration data. This adjustment of about 0.2 nm shortward reduced the TOMS derived ozone by 3–4 percent bringing it into better agreement with other satellite measurements, as well as Dobson.

Comparisons with a mid-northern latitude Dobson network indicate no significant trend in a bias of 0.5 percent in ozone with a standard deviation of 0.7 percent. The Version 7 TOMS ozone data set is independent of SBUV, and shows upward drifts at mid and low latitudes of 2 percent and 3 percent, respectively over the 11.5 years of useful lifetime of SBUV. This latitude dependence is consistent with uncertainties in the TOMS calibration, but the drifts are larger than the uncertainties in the TOMS calibration. A re-examination of the SBUV long-term calibration is warranted.

A small correction was made for "toggling" effects arising from intermittent changes in the state of synchronization between the TOMS chopper wheel and counting electronics. Larger instrumental errors associated with loss of synchronization are identified in the telemetry as "non-sync." These errors are mostly screened in the TOMS algorithms, and have little or no effect on the TOMS data archive.

The Version 7 data should be used in all future studies involving TOMS ozone or reflectivity.

ACKNOWLEDGMENTS

The TOMS and SBUV data presented in this report were prepared by the Ozone Processing Team (OPT) of NASA/ Goddard Space Flight Center. The data are archived and distributed by the Distributed Active Archive Center (DAAC) at the Goddard Space Flight Center in Greenbelt, Maryland. The Dobson data were received from the World Ozone Data Center, Atmospheric Environment Service, Toronto, Canada. The work was supported by NASA/ Goddard Space Flight Center under contract number NAS5-31755.

REFERENCES

Beckman Instruments, Final Report: Solar Backscatter Ultraviolet/Total Ozone Mapping Spectrometer (SBUV/TOMS) Program, Volume I, Technical Report, 1980, NASA Contract No. NAS5-20970.

Bhartia, P. K., J. R. Herman, R. D. McPeters, and O. Torres, 1994, "Effect of Mount Pinatubo on Total Ozone Measurements From Backscatter Ultraviolet (BUV) Experiments," *J. Geophys. Res., 98*, 18547-18554.

Bhartia, P. K., S. Taylor, R. D. McPeters, and C. Wellemeyer, 1995, "Application of the Langley Plot Method to the Calibration of the Solar Backscattered Ultraviolet Instrument on the Nimbus-7 Satellite," *J. Geophys. Res., 100*, 2997-3004.

Cebula, R. P., H. Park, and D. F. Heath, 1988, "Characterization of the Nimbus-7 SBUV Radiometer for the Long-Term Monitoring of Stratospheric Ozone," *J. Atm. Ocean. Tech., 5*, 215-227.

Fleig, Albert J., Pawan K. Bhartia, Charles G. Wellemeyer, and David S. Silberstein, 1986, "Seven Years of Total Ozone From the TOMS Instrument—A Report on Data Quality," *Geophys. Res. Lett., 13*, 1355-1358.

Fleig, Albert J., R. D. McPeters, P. K. Bhartia, Barry M. Schlesinger, Richard P. Cebula, K. F. Klenk, Steven L. Taylor, and D. F. Heath, 1990, "Nimbus-7 Solar Backscatter Ultraviolet (SBUV) Ozone Products User's Guide," *NASA Reference Publication, 1234*, National Aeronautics and Space Administration, Washington, DC.

Gleason, J. F., P. K. Bhartia, J. R. Herman, R. McPeters, P. Newman, R. S. Stolarski, L. Flynn, G. Labow, D. Larko, C. Seftor, C. Wellemeyer, W. D. Komhyr, A. J. Miller, and W. Planet, 1993, "Record Low Global Ozone in 1992," *Science, 260*, 523-526.

Heath, D. F., A. J. Krueger, H. R. Roeder, and B. D. Henderson, 1975, "The Solar Backscatter Ultraviolet and Total Ozone Mapping Spectrometer (SBUV/TOMS) for Nimbus G," *Opt. Eng., 14*, 323-331.

Heath, D., A. J. Krueger, and H. Park, 1978, "The Solar Backscatter Ultraviolet (SBUV) and Total Ozone Mapping Spectrometer (TOMS) Experiment," *The Nimbus-7 User's Guide*, edited by C. R. Madrid, pp. 175-211.

Herman, J. R., R. Hudson, R. McPeters, R. Stolarski, Z. Ahmad, X.-Y. Gu, S. Taylor, and C. Wellemeyer, 1991, "A New Self-Calibration Method Applied to TOMS/SBUV Backscattered Ultraviolet Data To Determine Long-Term Global Ozone Change," *J. Geophys. Res., 96*, 7531-7545.

Herman, J. R. and D. Larko, 1993, "Ozone Depletion at Northern and Southern Latitudes Derived From January 1979 to December 1991 Total Ozone Mapping Spectrometer Data," *J. Geophys. Res., 98*, 12783-12793.

Hilsenrath, E., R. P. Cebula, M. T. DeLand, K. Laamann, S. Taylor, C. Wellemeyer, and P. K. Bhartia, 1995, "Calibration of the NOAA-11 Solar Backscatter Ultraviolet (SBUV/2) Ozone Data Set From 1989 to 1993 Using In-Flight Calibration Data and SSBUV," *J. Geophys. Res., 100*, 1351-1366.

Hughes STX Corporation, 1994, "Nimbus-7 TOMS Wavelength Scale Adjustments," *Hughes STX Doc. HSTX-3036-212-MD-94-007*.

Jaross, G., A. Krueger, R. P. Cebula, C. Seftor, U. Hartmann, R. Haring, and D. Burchfield, 1995, "Calibration and Post-Launch Performance of the Meteor-3/TOMS Instrument," *J. Geophys. Res., 100*, 2985-2995.

Komhyr, W. D., R. D. Grass, and R. K. Leonard, 1989," Dobson Spectrophotometer 83: A Standard for Total Ozone Measurements, 1962-1987," *J. Geophys. Res., 94*, pp. 9847-9861.

McPeters, R. D., A. J. Krueger, P. K. Bhartia, J. R. Herman, A. Oaks, Z. Ahmad, R. P. Cebula, B. M. Schlesinger, T. Swissler, S. L. Taylor, O. Torres, and C. G. Wellemeyer, 1993, "Nimbus-7 Total Ozone Mapping Spectrometer (TOMS) Data Product's User's Guide," *NASA Ref. Publ. 1323*, National Aeronautics and Space Administration, Washington, DC.

McPeters, R. D., et al., 1996, "Nimbus-7 Total Ozone Mapping Spectrometer (TOMS) Data Product's User's Guide," *NASA Ref. Publ. Planned*, National Aeronautics and Space Administration, Washington, DC.

Paur, R. J., and A. M. Bass, 1985, "The Ultraviolet Cross-Sections of Ozone: II. Results and Temperature Dependence," *Atmospheric Ozone*, Edited by C. S. Zerefos and A. Ghazi, 611-616, D. Reidel, Dordrecht.

Schlesinger, B. M. and R. P. Cebula, 1992, "Solar Variation 1979-1987 Estimated From an Empirical Model for Changes With Time in the Sensitivity of the Solar Backscatter Ultraviolet Experiment", *J. Geophys. Res., 97*, 10119-10134.

Schoeberl, M. R., P. K. Bhartia, E. Hilsenrath, and O. Torres, 1993, "Tropical Ozone Loss Following the Eruption of Mt. Pinatubo," *Geophys. Res. Lett., 20*, 29-32.

Stolarski, R. S., R. Bojkov, L. Bishop, C. Zerefos, J. Staehelin, and J. Zawodny, 1992, "Measured Trends in Stratospheric Ozone," *Science 256*, 342-349.

Willson, R. C., H. S. Hudson, C. Frolich, and R. W. Brusa, 1986, "Long-Term Downward Trend in Solar Irradiance," *Science 234*, 1114-1117.

ACRONYM LIST

BRDF	Bi-directional Reflectivity Distribution Function
DAAC	Distributed Active Archive Center
FOV	Field of View
IFOV	Instantaneous Field of View
PJM	Pair Justification Method
PMT	Photo Multiplier Tube
SBUV	Solar Backscatter Ultraviolet
SSBUV	Space Shuttle Backscatter Ultraviolet
TOMS	Total Ozone Mapping Spectrometer

REPORT DOCUMENTATION PAGE

Form Approved
OMB No. 0704-0188

1. AGENCY USE ONLY *(Leave blank)*	2. REPORT DATE	3. REPORT TYPE AND DATES COVERED
	March 1996	Contractor Report

4. TITLE AND SUBTITLE

Final Report on Nimbus–7 TOMS Version 7 Calibration

5. FUNDING NUMBERS

Code 916
Contract NAS5-31755

6. AUTHOR(S)

C. G. Wellemeyer, S. L. Taylor, G. Jaross, M. T. DeLand, C. J. Seftor,
G. Labow, T. J. Swissler, and R. P. Cebula

7. PERFORMING ORGANIZATION NAME(S) AND ADDRESS(ES)

Hughes STX Corporation
Greenbelt, MD 20770

8. PERFORMING ORGANIZATION REPORT NUMBER

GSFC: 96B00048

HSTX-3036-501-CW-96-003

9. SPONSORING/MONITORING AGENCY NAME(S) AND ADDRESS(ES)

NASA Aeronautics and Space Administration
Washington, D.C. 20546-0001

10. SPONSORING/MONITORING AGENCY REPORT NUMBER

CR-4717

11. SUPPLEMENTARY NOTES

C. G. Wellemeyer, S. L. Taylor, G. Jaross, M. T. DeLand, C. J. Seftor,
G. Labow, T. J. Swissler, and R. P. Cebula: Hughes STX Corporation, Greenbelt, Maryland

12a. DISTRIBUTION/AVAILABILITY STATEMENT

Unclassified-Unlimited
Subject Category: 46
This report is available from the NASA Center for AeroSpace Information,
800 Elkridge Landing Road, Linthicum Heights, MD 21090; (301) 621-0390.

12b. DISTRIBUTION CODE

13. ABSTRACT *(Maximum 200 words)*

This report describes an improved instrument characterization used for the Version 7 processing of the Nimbus–7 Total Ozone Mapping Spectrometer (TOMS) data record. An improved internal calibration technique referred to as spectral discrimination is used to provide long-term calibration precision of ±1%/decade in total column ozone amount. A revised wavelength scale results in a day one calibration that agrees with other satellite and ground-based measurements of total ozone, while a wavelength independent adjustment of the initial radiometric calibration constants provides good agreement with surface reflectivity measured by other satellite-borne ultraviolet measurements. The impact of other aspects of the Nimbus–7 TOMS instrument performance are also discussed. The Version 7 data should be used in all future studies involving the Nimbus–7 TOMS measurements of ozone. The data are available through the NASA Goddard Space Flight Center's Distributive Active Archive Center (DAAC).

14. SUBJECT TERMS

ozone, stratospheric, Nimbus 7, TOMS (Total Ozone Mapping Spectrometer), instrument, calibration

15. NUMBER OF PAGES

54

16. PRICE CODE

17. SECURITY CLASSIFICATION OF REPORT	18. SECURITY CLASSIFICATION OF THIS PAGE	19. SECURITY CLASSIFICATION OF ABSTRACT	20. LIMITATION OF ABSTRACT
Unclassified	Unclassified	Unclassified	Unlimited

National Aeronautics and
Space Administration
Code JTT
Washington, D.C.
20546-0001

Official Business
Penalty for Private Use, $300